

## Micelles of Lipid–Oligonucleotide Conjugates: Implications for Membrane Anchoring and Base Pairing

C. Gosse,<sup>\*,†,‡,§</sup> A. Boutorine,<sup>||</sup> I. Aujard,<sup>‡</sup> M. Chami,<sup>#,⊥</sup> A. Kononov,<sup>‡</sup> E. Cogné-Laage,<sup>‡</sup> J.-F. Allemand,<sup>\*,†,‡</sup> J. Li,<sup>‡</sup> and L. Jullien<sup>\*,‡</sup>

Laboratoire de Physique Statistique CNRS UMR 8550, Ecole Normale Supérieure, 24 rue Lhomond, F-75231 Paris Cedex 05, France, Département de Chimie CNRS UMR 8640, Ecole Normale Supérieure, 24 rue Lhomond, F-75231 Paris Cedex 05, France, Laboratoire de Biophysique CNRS/MNHN UMR 5153, Muséum National d'Histoire Naturelle, 43 rue Cuvier, F-75231 Paris Cedex 05, France, and Laboratoire de Physico-Chimie CNRS UMR 168, Institut Curie, 26, rue d'Ulm, 75248 Paris Cedex 05, France

Received: October 27, 2003; In Final Form: February 23, 2004

This report examines the organization properties of new fluorescent DNA-lipids, either alone in water or in interaction with 1-octyl- $\beta$ -D-glucopyranoside micelles or egg phosphatidylcholine vesicles. We first describe the design and the syntheses of the conjugates. Then, we use UV–Vis absorption, steady-state fluorescence emission, electron microscopy, and fluorescence correlation spectroscopy after two-photon excitation to show that these DNA-lipids form spherical micelles in aqueous solution and incorporate much better in micelles than in vesicles. We also investigate the significance of the lipophilic chains of these DNA-lipids on the melting behavior of the double-stranded hybrids: in water melting curves are broadened whereas in amphiphilic assemblies duplexes melt as the unconjugated controls. This work is expected to be useful for improving the rational design of antisense medicines.

### Introduction

DNA oligonucleotides recently emerged as useful building blocks to obtain self-assembled arrays such as large organized molecular crystals.<sup>1</sup> Indeed, they only exhibit strong intermolecular association when their sequences are complementary. In view of these attractive features, we have been interested to use the DNA strategy to design bidimensional polymeric networks<sup>2,3</sup> reminiscent of biological structures.<sup>4–7</sup> To restrict cross-linking in two dimensions, we decided to rely on a 2D template,<sup>7–12</sup> i.e., the surface of lipid vesicles, to polymerize amphiphilic monomers made of oligonucleotides.

The prerequisite to achieve the preceding goal was to design and synthesize DNA-lipids (IDNAs) able to incorporate within bilayer cores. Such an issue is closely related to the improvement of the cellular uptake of antisense oligonucleotides by lipophilic modification.<sup>13–15</sup> According to this therapeutic strategy, short single-stranded DNA (ss-DNA) first bind to cellular membrane because of their hydrophobic moiety; then, after internalization, they hybridize to the targeted mRNA by sequence recognition and consequently prevent the translation of the associated protein. Oligonucleotides have been conjugated to numerous small lipophilic molecules including the widely used cholesterol,<sup>13,16–18</sup> alkyl chain,<sup>16,19</sup> di-*o*-alkyl-*rac*-glycerol,<sup>15,16</sup> fullerene,<sup>20</sup> and adamantane.<sup>15</sup> Biological effects such as inhibition of viral protein expression by lipid-conjugates could be observed on cell

cultures, but the mechanisms ruling drug action are still unclear.<sup>15,21</sup> Indeed, cholesterol-DNA was found to bind to low-density lipoproteins receptors, allowing an alternative internalization route to passive membrane anchoring followed by pinocytosis.<sup>14</sup> Moreover, drug activity does not always correlate with a specific sequence, suggesting mechanisms other than antisense inhibition.<sup>15,21</sup>

Although lots of efforts have been devoted to IDNA synthesis and pharmaceutical characterization, data concerning the physicochemical properties of such amphiphiles are scarce.<sup>17,18</sup> Consequently, the present report investigates several features of newly synthesized IDNAs bearing a fluorescent label in their hydrophobic moiety. The manuscript first exposes the design and the syntheses of the fluorescent IDNAs. Subsequently, the phase behavior of these conjugates, alone in aqueous solution, or in the presence of organized assemblies such as micelles or vesicles, was studied by fluorescence spectroscopy and electron microscopy. Finally, we tried to analyze the influence of the location of the lipophilic chains, i.e., in water or in amphiphilic assemblies, on the melting behavior of the double-stranded hybrids.

### Results and Discussion

**Design and Syntheses of DNA-Lipids.** In relation with the initial goal of building a 2D-polymeric network, we considered the stepwise temperature-controlled polycondensation of a DNA network on a lipid bilayer. Each monomer was designed as a core DNA duplex bearing a lipophilic anchor and three single-stranded dangling oligonucleotides at its extremities (see Supporting Information; Figure 1S). More precisely, such an assembly was aimed to be obtained by hybridization between a long unmodified strand (ACA or A'CA') and a lipophilic conjugate (IGeB or IGeB'; see Scheme 2 for conjugate formula and Experimental Section for detailed sequences). Central core sequences (C and G) were chosen to pair at any temperature below 50 °C and distal sequences (A and A' or B and B') to reticulate complementary monomers only around 30 °C. In the

\* To whom correspondence should be addressed. E-mail: charlie.gosse@lpn.cnrs.fr. Tel: 33 1 69 63 61 55. Fax: 33 1 69 63 60 06; E-mail: Jean-Francois.Allemand@ens.fr. Tel: 33 1 44 32 34 92; Fax: 33 1 44 32 34 33. E-mail: Ludovic.Jullien@ens.fr. Tel: 33 1 44 32 33 33; Fax: 33 1 44 32 33 25.

† CNRS UMR 8550, Ecole Normale Supérieure.

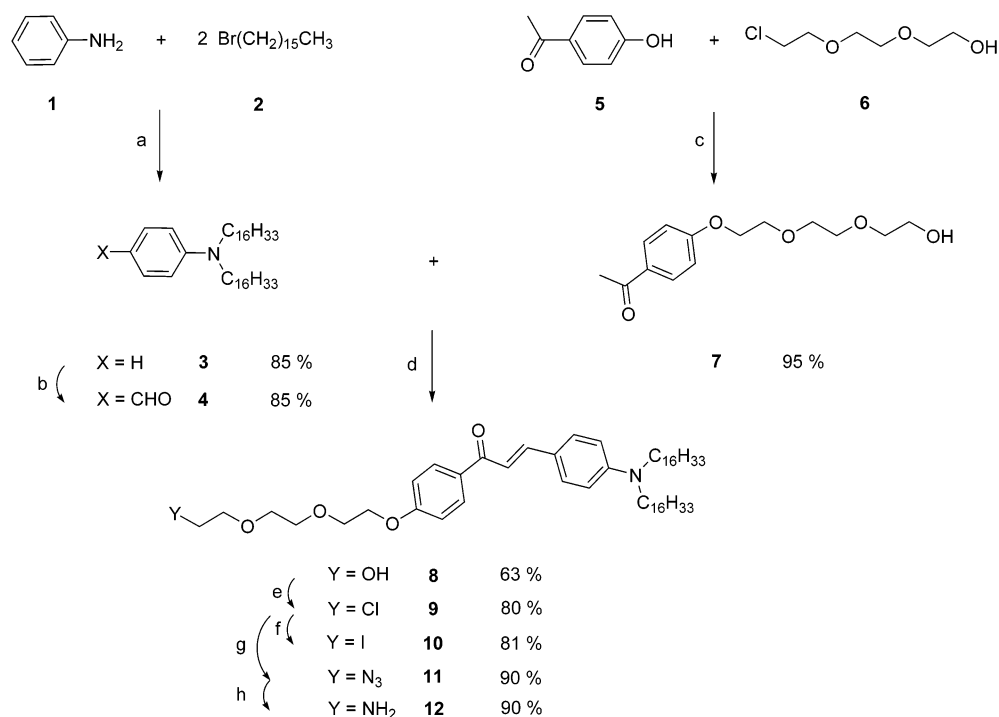
‡ CNRS UMR 8640, Ecole Normale Supérieure.

|| CNRS/MNHN 5153, Muséum National d'Histoire Naturelle.

# CNRS UMR 168, Institut Curie.

§ Present address: CNRS/LPN, Laboratoire de Photonique et de Nanostructures, Route de Nozay, 91460 Marcoussis, France.

⊥ Present address: M. E. Müller Institute (MSB), Biozentrum, University of Basel, Klingelbergstr. 70 CH-4056 Basel, Switzerland.

SCHEME 1<sup>a</sup>

<sup>a</sup> (a) K<sub>2</sub>CO<sub>3</sub>, *n*-BuOH, 110 °C, 72 h; (b) POCl<sub>3</sub>, DMF, 100 °C, 3 h; (c) K<sub>2</sub>CO<sub>3</sub>, KI, *n*-BuOH, 110 °C, 12 h; (d) KOH, EtOH/CH<sub>2</sub>Cl<sub>2</sub> 1/1, 35 °C, 48 h; (e) P(Ph)<sub>3</sub>, imidazole, CCl<sub>4</sub> reflux, 3 h; (f) NaI, 2-butanone reflux, 48 h; (g) NaN<sub>3</sub>, DMF, 80 °C, 12 h; (h) P(Ph)<sub>3</sub>, H<sub>2</sub>O, THF, 24 h.

TABLE 1: Solvatochromism of the Chalcone Chromophore<sup>a</sup>

solvent	chalcone substrate	dielectric constant <sup>b</sup>	$\lambda_{\max}$ (nm)	$\lambda_{\text{em}}(\lambda_{\text{exc}})$ (nm)
ethyl acetate	<b>8</b>	6	416	492 (426)
tetrahydrofuran	<b>8</b>	8	408	484 (418)
methylene chloride	<b>8</b>	9	424	518 (434)
acetone	<b>8</b>	21	418	513 (428)
ethanol	<b>8</b>	25	427	556 (437)
dimethylformamide	<b>8</b>	37	425	523 (435)
dimethyl sulfoxide	<b>8</b>	46	430	533 (440)
H <sub>2</sub> O <sup>c</sup>	<b>IGeB</b>	78	430	559 (430)
H <sub>2</sub> O <sup>c</sup>	<b>IGeB'</b>	78	429	560 (430)
OG micelles in H <sub>2</sub> O <sup>d</sup>			419	530 (430)
EPC vesicles in H <sub>2</sub> O <sup>e</sup>	<b>IGeB</b>			551 (430)
EPC vesicles in H <sub>2</sub> O <sup>e</sup>	<b>IGeB'</b>			555 (430)

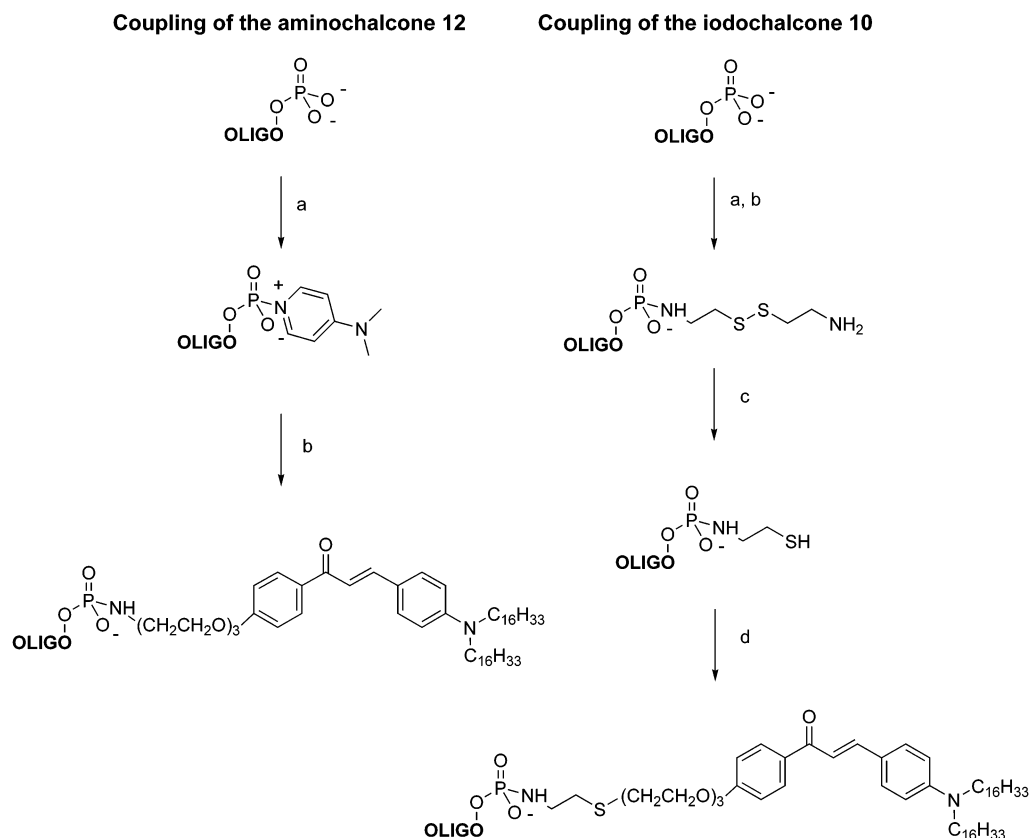
<sup>a</sup> Wavelengths of the maxima of absorption ( $\lambda_{\max}$ ) and emission ( $\lambda_{\text{em}}$ ; excitation at  $\lambda_{\text{exc}}$ ) in different solvents. Measurements were performed at 298 K at micromolar concentrations. <sup>b</sup> Values extracted from ref 30. <sup>c</sup> 100 mM NaCl, 10 mM Na(CH<sub>3</sub>)<sub>2</sub>AsO<sub>2</sub>-HCl, pH 7 buffer. <sup>d</sup> [OG] = 20 mM in 100 mM NaCl, 10 mM Na(CH<sub>3</sub>)<sub>2</sub>AsO<sub>2</sub>-HCl pH 7 buffer. <sup>e</sup> [EPC] = 1.2 mM in 100 mM NaCl, 10 mM Na(CH<sub>3</sub>)<sub>2</sub>AsO<sub>2</sub>-HCl pH 7 buffer.

previous notations, **1** is a chalcone fluorophore-bearing lipid, and **e** is a tri(ethylene-glycol) spacer that had to be introduced for preventing interactions between 3' and 5' dangling strands facing each other at the duplex end (Table 1S). The chalcone motif was selected as a polarity fluorescent reporter in relation to its favorable photophysical properties and easy synthetic access (vide infra).

The fluorescent lipid backbone **1** was first synthesized (Scheme 1). Dialkylation of aniline **1** was performed by bromohexadecane **2** in *n*-butanol.<sup>22</sup> The resulting *N,N*-dihexadecyl aniline **3** was converted to 4-*N,N*-dihexadecylaminobenzaldehyde **4** by the Vilsmeier–Haack reaction.<sup>23</sup> The acetophenone unit **7** was prepared from alkylation of the para-hydroxyacetophenone **5** with 2-[2-(2-chloroethoxy)ethoxy]-ethanol **6** in *n*-butanol in the presence of potassium carbonate and potassium iodide. The key reaction to build the chalcone chromophore is

the condensation of acetophenone derivatives on aldehydes. It is generally performed in alcohols sometimes mixed with water. Basic conditions are generally used for the condensation.<sup>24,25</sup> Catalytic amounts of bases were surprisingly not sufficient to afford satisfactory yields; instead, stoichiometric amounts were used as already reported.<sup>25,26</sup> Aldehydes parasubstituted with electron donating groups such as amine are deactivated and lead to modest yields as observed in the present case in agreement with the literature.<sup>26,27</sup> Thus, **4** and **7** were condensed under basic conditions (progressive addition of potassium hydroxide) in a mixture of ethanol and methylene chloride to yield the chalcone hydroxy-terminated lipid **8**. The latter was then converted into the corresponding chloride **9** using triphenylphosphine and imidazole in carbon tetrachloride.<sup>28</sup> **9** was eventually transformed either into the iodide derivative **10** by refluxing in butanone in the presence of potassium iodide, or into the amino derivative **12** after triphenyl phosphine reduction of the azido derivative **11** resulting from substitution of chloride by sodium azide in DMF.

IDNAs were obtained from coupling between the appropriate oligonucleotides and the fluorescent lipid backbone. Two different coupling procedures were investigated (Scheme 2).<sup>29</sup> In the first, conjugate is obtained by reaction between the activated 5' terminal phosphate of the oligonucleotide and the amino lipid **12**. The second way of synthesis included attachment of a cysteamine moiety to the terminal 5' phosphate, reduction of the product by dithiothreitol to generate a terminal sulfhydryl group, and alkylation of this group by the iodide chalcone **10**. The presently investigated IDNA, **IGeB** and **IGeB'**, were obtained using the second procedure; however, no essential differences were found between conjugates whatever the synthetic route followed. Moreover, we would like to point out that classical acrylamide gel or reverse phase HPLC purifications were not possible due to the aggregation of IDNA in micelles (vide infra). Consequently, as for fullerene conjugates,<sup>20</sup> mixed

SCHEME 2<sup>a</sup>

<sup>a</sup> (a) P(Ph)<sub>3</sub>, dipyridyl disulfide, DMAP, DMSO, 15 min; (b) RNH<sub>2</sub>, TEA, DMSO, 2 h; (c) DTT, Tris HCl pH 7.5, 1 h; (d) RI, TEA, pyridine, 12 h. The lipid backbone is designated by the short-hand I in the text. See Experimental Section for detailed oligonucleotide sequences.

Triton X-100/IDNA micelles were purified on agarose, resulting in a relatively low overall yield (~10%).

**Investigation of the Photophysical Properties of the Chalcone Chromophore as a Fluorescent Label.** The significance of solvatochromism on absorption and emission features of the chalcone chromophore was first examined on the model chalcone lipid **8** (Table 1). The organic solutions of **8** are yellow (absorption in the 400–430 nm range) and emit a strong green fluorescence (480–560 nm). The observed positive solvatochromism, i.e., the spectra red shift with rising solvent polarity, is indicative of an increase of the dipolar molecular moment upon light absorption;<sup>30</sup> it conforms to the reported features from different 4-amino phenyl-substituted chalcones.<sup>31</sup> This behavior made suitable the use of the synthesized chromophore as a polarity-sensitive fluorescent label<sup>32</sup> for investigating the partition properties of **IGeB** and **IGeB'** between the aqueous phase and organized assemblies.<sup>33</sup>

**Supramolecular Organization of DNA-Lipids in Aqueous Solution.** In the micromolar range, **IGeB** and **IGeB'** gave yellow nondiffusing aqueous solutions at room temperature in 100 mM NaCl, 10 mM Na(CH<sub>3</sub>)<sub>2</sub>AsO<sub>2</sub>-HCl pH 7 buffer. The red-shifted maxima for the chalcone absorption and emission (Table 1) suggested that the chromophore was surrounded by a polar medium. These observations supported at first sight that these IDNAs were monomeric in water. To control the latter, a 2.5 μM **IGeB** solution was examined by electron microscopy (EM). Numerous small spherical aggregates (diameter range: 8–15 nm) were distinctly observed (Figure 1b), suggesting the presence of small micelles made of pure **IGeB**. Because the conditioning of the samples for EM observation could promote the formation of the micelles, we independently investigated the structure of the **IGeB** solution by measuring the lateral

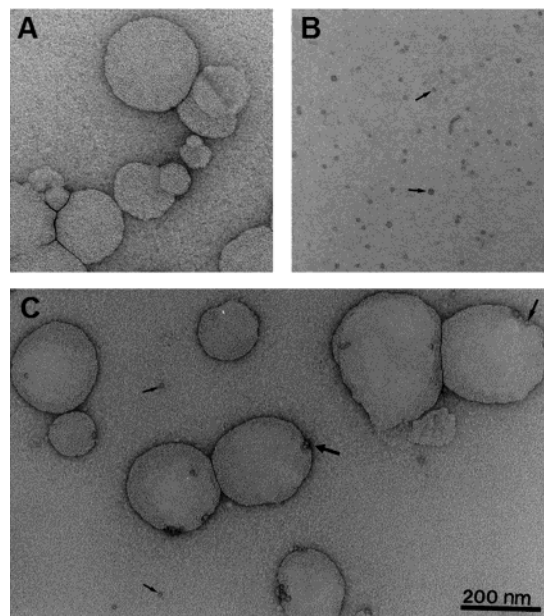


**Figure 1.** Titration of 2.5 μM **IGeB** by EPC vesicles as observed by electron microscopy. (a) control experiment: EPC vesicles alone ([EPC] = 18 mM); (b) [EPC] = 0 mM; (c) [EPC] = 18 mM.

diffusion coefficient of the conjugate in diluted solutions. Indeed, diffusion coefficients are sensitive to the shape and size of the diffusing objects; thus, they can be fruitfully used to evidence the formation of any aggregates.<sup>34,35</sup> In view of the low amounts of available material and of the intrinsic fluorescence of the present chalcone, fluorescence correlation spectroscopy (FCS)<sup>36</sup> was the technique selected for this experiment.<sup>37</sup> The diffusion

coefficients measured at 293 K were converted into hydrodynamic radii by using the Stokes law (see Experimental Section, eq 8) that accounts for an isotropic reorientation of the objects. At 10 nM, the apparent hydrodynamic radius of **IGeB** in 100 mM NaCl, 10 mM Tris-HCl pH 7 buffer was found to be equal to  $11 \pm 2$  nm using the reported 2.7 nm hydrodynamic radius of 1-octyl- $\beta$ -D-glucopyranoside (OG) micelles<sup>38</sup> for calibration (vide infra). This value strongly exceeded the molecular size of **IGeB** but was in fair agreement with the size of the aggregates observed by EM. It supported that **IGeB** spontaneously forms stable micelles at concentrations as low as a 10 nM. Assuming that nucleotidic strands are spheres, approximately 2 nm in radius,<sup>37</sup> which are compactly arranged at the aggregate surface, we can estimate a crude average number of IDNAs per micelle of about 20. In relation to solvatochromism, the large polarity of the micellar core of **IGeB** could express a poor packing of alkyl chains and a resulting hydrophobic center rather open to the penetration of water molecules.

Despite the large volume of the DNA headgroup and the possible attractive interactions between the dangling nucleic bases and the alkyl chains, **IGeB** gives micelles exhibiting a 10 nM upper limit of the critical micellar concentration (CMC). Studies on cholesterol conjugated 10mers reported either a 150  $\mu$ M CMC<sup>17</sup> or no CMC at all below 1 mM.<sup>18</sup> This large difference with our CMC value can be interpreted as a consequence of the marked hydrophobic nature of the chalcone lipid used here. Indeed, if we roughly consider that lipid **8** is equivalent to a cholesterol molecule plus two C<sub>16</sub> alkyl chains, the two CMC should differ, following theoretical derivations, by a factor 2<sup>16</sup> i.e.,  $\sim 65000$ .<sup>39</sup>

At 293 K, the equilibrium constant  $K_{w \rightarrow pm}$  characterizing **IGeB** partition between the buffer and the pure **IGeB** micellar phase (respectively denoted w and pm in subscript):

$$\text{IGeB (buffer)} = \text{IGeB (IGeB micelles)} \quad (1)$$

is thus larger than  $\text{CMC}^{-1}$ ,<sup>39</sup> that is  $10^8$ .<sup>40</sup> This result bears much significance for optimizing the partition coefficients of IDNAs between the aqueous phase and organized assemblies such as vesicles. In fact, anchoring of the lipid backbone within hydrophobic cores was anticipated as the major driving force for favoring extraction from water. However, in the present system, lipid chains are buried inside micelles, already kept out of contact with water molecules. Consequently, weaker entropic considerations arising from lateral steric interactions between headgroups of IDNAs and involving the curvature of the organized medium will probably represent the only driving force that controls incorporation in other organized assemblies.

**Partition of DNA-Lipids between Water and 1-Octyl- $\beta$ -D-glucopyranoside Micelles.** The interaction between the IDNAs and OG was first approached by titration of 3  $\mu$ M **IGeB'** by 200 mM OG in 100 mM NaCl, 10 mM Na(CH<sub>3</sub>)<sub>2</sub>AsO<sub>2</sub>-HCl pH 7 buffer at 293 K. Figure 2 display the results of this experiment followed by UV-Vis absorption and steady-state fluorescence emission spectroscopies. The absorbance of **IGeB'** decreased and became blue-shifted after addition of the first aliquot of OG solution; then, one observed a monotonic increase of extinction at larger OG concentrations. Meanwhile, the fluorescence emission first increased and became blue-shifted up to OG concentrations lying in the range of its critical micellar concentration (25 mM in water at 298 K<sup>38</sup>); beyond this concentration, it did not evolve anymore. Similar observations were made with **IGeB**. They can be explained on the basis of the phase behavior of OG molecules that, below their CMC, at least partially anchor into micelles initially made of pure **IGeB'**.

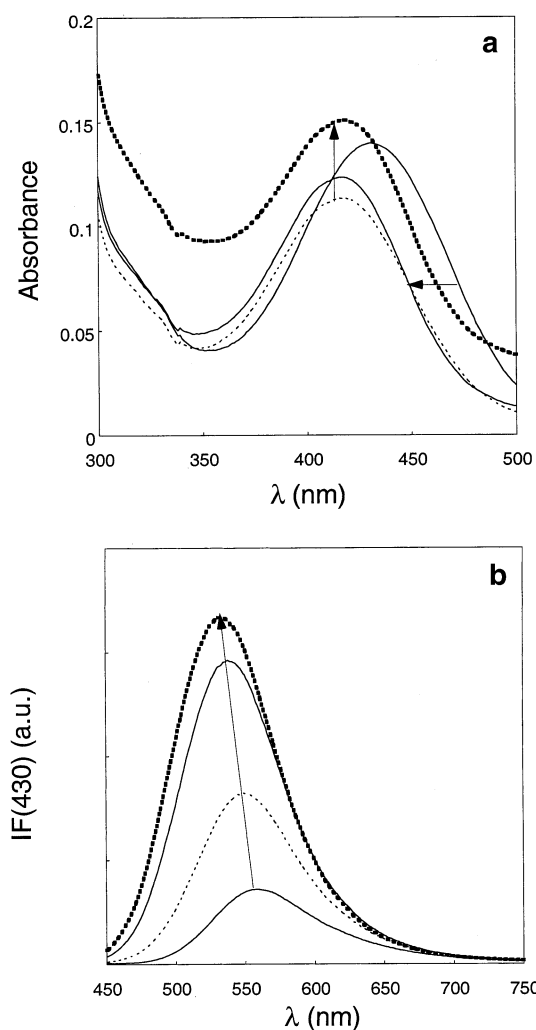


**Figure 2.** Titration of **IGeB'** (450  $\mu$ L; initial concentration 3  $\mu$ M) by 1-octyl- $\beta$ -D-glucopyranoside (titrating solution: 200 mM) in 100 mM NaCl, 10 mM Na(CH<sub>3</sub>)<sub>2</sub>AsO<sub>2</sub>-HCl pH 7 buffer at 293 K. (a) Evolution of the absorption spectra after addition of 0  $\mu$ L (thin solid line), 20  $\mu$ L (thin dotted line), 40  $\mu$ L (thin solid line), and 60  $\mu$ L (thick dotted line; corresponds to OG CMC) of titrating solution; (b) Evolution of the emission spectra ( $\lambda_{\text{exc}} = 430$  nm) after addition of 0  $\mu$ L (thin solid line), 20  $\mu$ L (thin dotted line), 40  $\mu$ L (thin solid line), 60  $\mu$ L (thick dotted line; corresponds to OG CMC) of titrating solution.

Following this assumption, the consequences should be 2-fold. First, the average distance between IDNA molecules is increased, leading to decrease the short-range strong electronic coupling<sup>41</sup> existing between chalcone chromophores initially at close contact. Although difficult to quantitatively evaluate in the absence of a satisfactory description of the relative orientation and distance between the transition dipole moments in initial micelles, the absorption alteration in the very first stages of the present titration (blue- and hypsochromic shift) could be typically observed.<sup>34</sup> Second, addition of cone-shaped OG molecules is anticipated to render the micellar core less permeable to water molecules, and thus more hydrophobic, by better accommodating smooth micellar shapes. In view of the solvatochromic chalcone behavior, blue-shifts in absorption and emission should be observed as in the present case (Table 1). In addition, the corresponding increase of fluorescence quantum yield of the chalcone chromophore during titration conforms to the reported behavior of 4-dimethylaminochalcone interacting with several detergents.<sup>42</sup> Finally, above OG CMC, increasing amounts of OG micelles are formed; they induce light scattering, promoting the increase of extinction observed in Figure 2a. In

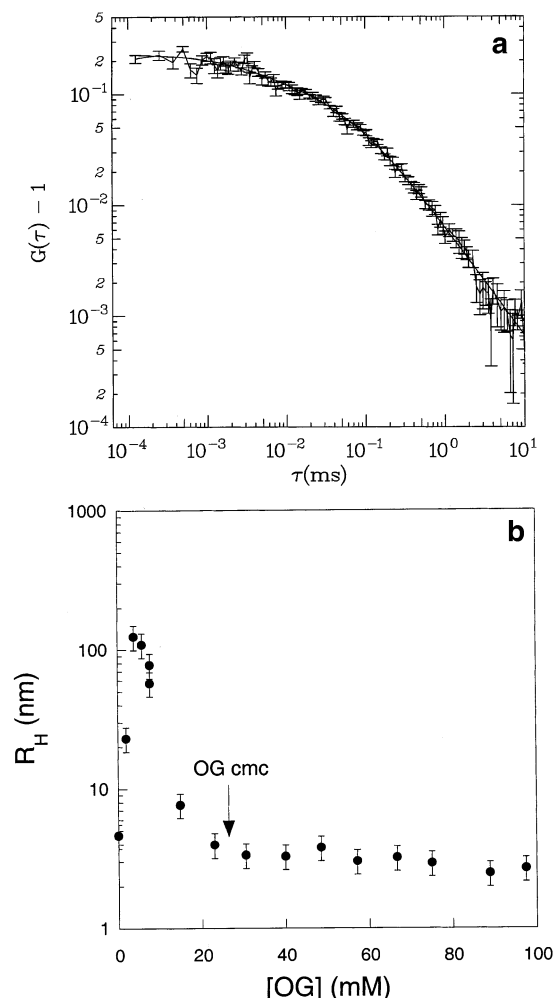


**Figure 3.** (a) Autocorrelation curve recorded at 293 K from a solution 10 nM in **IGeB** and 23 mM in OG ( $\lambda_{\text{exc}} = 780$  nm) leading to  $\tau_D = 36$   $\mu\text{s}$ ; (b) Evolution of the hydrodynamic radius  $R_H$  as extracted from the titration by FCS of **IGeB** (10 nM) by 1-octyl- $\beta$ -D-glucopyranoside (titrating solution: 200 mM) in 100 mM NaCl, 10 mM Tris-HCl/Tris pH 7 buffer.

contrast, no major evolution is observed in fluorescence emission (Figure 2b), in line with the absence of influence of light scattering on the fluorescence intensity in the investigated OG concentration range.

The titration of a 10 nM **IGeB'** solution by 200 mM OG in 100 mM NaCl, 10 mM  $\text{Na}(\text{CH}_3)_2\text{AsO}_2\text{-HCl}$  pH 7 buffer was also followed by FCS at 293 K. Figure 3a displays a typical autocorrelation curve. Satisfactory fits were obtained during the whole titration by assuming a single purely diffusive behavior obeying eq 6 (see Experimental Section). This observation strongly suggested that the structures in solution were rather homogeneous at any step of the titration. The characteristic diffusion time  $\tau_D$  for crossing the excitation volume was extracted from each experimental curve by fitting, and it was converted after viscosity correction into a hydrodynamic radius  $R_H$  according to eqs 7 and 8 (see Experimental Section and Supporting Information, Figure 5Sa). Figure 3b displays the evolution of the hydrodynamic radius of **IGeB'**-containing organized assemblies as a function of OG concentration. The behavior is nonmonotonic: the hydrodynamic radius first increases sharply up to 4 mM in OG with spherical micelles of pure **IGeB'** being transformed in much larger assemblies. Then, in a second regime, the hydrodynamic radius drops quickly and stabilizes above OG CMC. An independent measurement

performed on OG micelles labeled with **8** at 10 nM provided the same value of the hydrodynamic radius as the asymptotic one observed in this second regime. Consequently, the whole  $R([\text{OG}])$  curve was calibrated using reported values of the hydrodynamic radius for OG micelles.<sup>38</sup>

The present observations suggest that mixtures of **IGeB'** and OG molecules give homogeneous lyotropic organized assemblies in the whole range of the investigated concentrations. Small micelles are present at both extremities of the corresponding phase diagram. In the intermediate regime in which OG is present below its CMC, one observes the formation of large assemblies<sup>43</sup> whose core is suggested to be more hydrophobic than the one of the initial **IGeB'** micelles, indicating a better packing of the hydrophobic moieties of the lipids. The absence of heterogeneity supported by FCS observations at 10 nM IDNA concentration allows us to evaluate an upper limit of  $10^8$  for the equilibrium constant  $K_{\text{pm} \rightarrow \text{mm}}$  at 293 K of **IGeB'** partition between the pure (pm) and the mixed micellar (mm) phases:

$$\text{IGeB}' (\text{IGeB}' \text{ micelles}) = \text{IGeB}' (\text{OG-IGeB}' \text{ micelles}) \quad (2)$$

**Partition of DNA-Lipids between Water and EPC Large Unilamellar Vesicles.** We used large unilamellar vesicles (LUV) made from egg phosphatidylcholine (EPC) to evaluate the partition of the present IDNAs between water and lipid bilayers. In a first series of experiments, we titrated 0.8  $\mu\text{M}$  **IGeB** by increasing amounts of 3.6 mM EPC LUV in 100 mM NaCl, 10 mM  $\text{Na}(\text{CH}_3)_2\text{AsO}_2\text{-HCl}$  pH 7 buffer at 293 K. Both the intensity and the steady-state anisotropy  $\langle r \rangle$  of fluorescence emission of the chalcone lipid were recorded as a function of EPC concentration up to 1.5 mM (Figure 4). As observed during the titration of the IDNAs by OG, addition of EPC vesicles promoted at the same time a blue-shift and an increase of the fluorescence emission of the chalcone. These features are in line with an increase of hydrophobicity of the chromophore surroundings upon titration. In addition, the steady-state emission anisotropy  $\langle r \rangle$  increased in the presence of EPC vesicles. This trend can be interpreted as a local increase in viscosity due to interaction between IDNA and EPC assemblies. Indeed, emission anisotropy  $\langle r \rangle$  expresses the depolarizing motions occurring during the lifetime  $\tau$  of the excited state.<sup>32</sup> As an example, the Perrin's relation

$$\frac{1}{\langle r \rangle} = \frac{1}{r_0} \left( 1 + \frac{\tau}{\tau_c} \right) \quad (3)$$

applies for isotropic rotations where  $r_0$  designates the fundamental anisotropy characteristic of the chromophore and  $\tau_c$  the molecular correlation time. The quantum yield of fluorescence was larger in the presence of EPC LUV, implying a longer lifetime of the excited state (those two parameters are proportional). Since both  $\langle r \rangle$  and  $\tau$  increased, we conclude that the correlation time of the chalcone chromophore also strongly increased in the presence of EPC LUV; the surrounding medium of the fluorescent label became more viscous upon vesicle addition. The same type of titration was performed with 7.1 mM EPC LUV labeled with 2% (mol/mol) rhodamine-phosphatidylethanolamine. Because of energy transfer of electronic excitation from the chalcone to the rhodamine, a decrease of the chalcone emission and an increase of the rhodamine one were simultaneously anticipated if the distance between both chromophores would drop sufficiently during the experiment.<sup>32</sup> Such a behavior was indeed observed (see Supporting Information, Figure 2Sa,b). It supports that mixed assemblies from **IGeB**

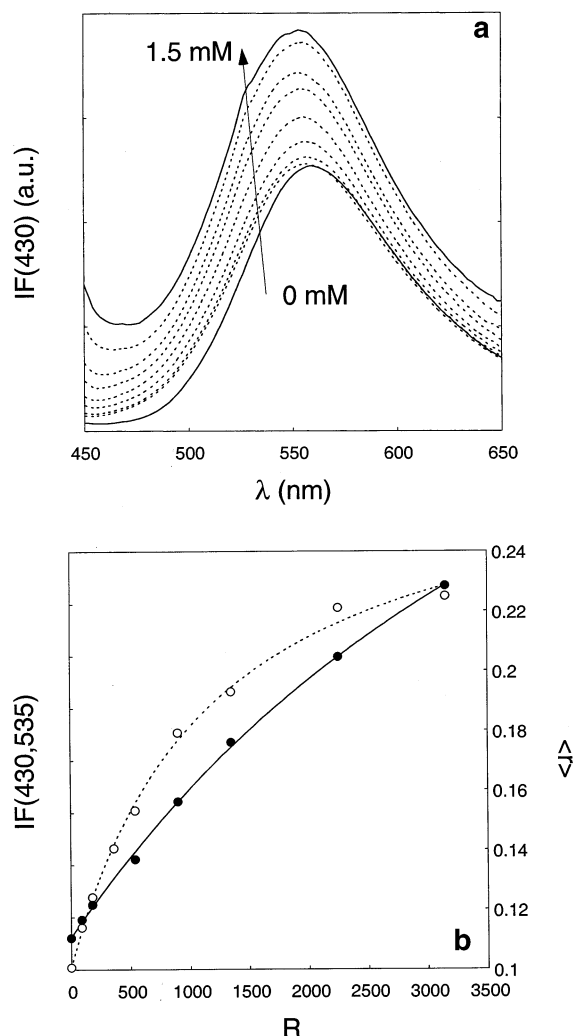
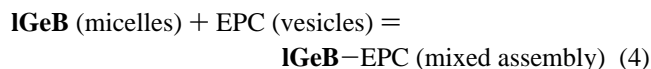


**Figure 4.** Titration of 0.8  $\mu\text{M}$  IGeB by 3.6 mM EPC LUV at 293 K. (a) Collection of steady-state emission spectra corrected from dilution upon excitation at 430 nm as a function of the EPC concentration of vesicle suspension; (b) Normalized fluorescence intensity  $I_F(430, 535)$  (empty circles) and steady-state emission anisotropy  $\langle r \rangle$  (filled circles) at 535 nm as a function of the ratio  $R = [\text{EPC}]_{\text{tot}}/[\text{IGeB}]_{\text{tot}}$ . The fits according to eq 9 are respectively displayed as dotted ( $I_F(430, 535)$ ) and solid ( $\langle r \rangle$ ) lines.  $\lambda_{\text{exc}} = 430$  nm. See Experimental Section.

and EPC LUV were formed. The experimental data were quantitatively analyzed by modeling the interaction between IGeB and EPC by the complexation reaction of equilibrium constant  $K_{\text{mix}}$ :<sup>44</sup>



Similar observations were made with IGeB', and Table 2 sums up the results for both IDNAs. Association constants  $K_{\text{mix}}$  in the 500–1500 range were found at 293 K. Hence, starting from a solution of micelles of IDNAs in the micromolar range, these evaluations suggested that incorporation in EPC vesicles would mainly occur over by  $[\text{EPC}] \approx 2\text{--}3$  mM.

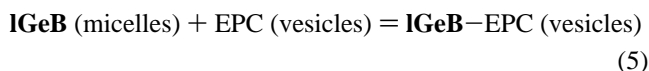
During our experiments, drawbacks of steady-state fluorescence spectroscopy were 2-fold: it could not be used at EPC concentrations larger than a few millimolar due to light scattering by LUVs, and it did not provide any global structural information on the sample. Therefore, we independently used electron microscopy to investigate IDNA partition. The morphology of IDNA-EPC mixed assemblies was examined upon titration of 2.5  $\mu\text{M}$  IGeB by EPC LUV up to  $[\text{EPC}] = 25$  mM:

**TABLE 2: Affinity Constants  $K_{\text{mix}}$  of the Conjugates for EPC Vesicles and Alteration of the Emissive Properties of the Chalcone Fluorophore during Fluorescence-Based Titration by LUVs ( $\lambda_{\text{exc}} = 430$  nm)<sup>a</sup>**

IDNA	$K_{\text{mix}}^b$	$I_F(\infty)/I_F(0)$ ( $\lambda_{\text{obs}}$ in nm <sup>c</sup> )
IGeB	$1300 \pm 500^d$	2.0 (535) <sup>d</sup>
	$400 \pm 200^e$	3.4 (535) <sup>e</sup>
	$1300 \pm 500^f$	0.6 (540) <sup>f</sup>
IGeB'	$800 \pm 400^d$	1.8 (535)

<sup>a</sup> See text and Experimental Section. <sup>b</sup> See eq 9; standard state: ideal solute at 1 M for the infinitely diluted solution; data collected at 293 K. <sup>c</sup> Wavelength at which data analysis was performed according to eq 9. <sup>d</sup> As evaluated from the evolution of the fluorescence intensity of the chalcone IDNA-lipid as a function of  $R$ . See eq 9. <sup>e</sup> As evaluated from the evolution of the steady-state emission anisotropy  $\langle r \rangle$  of the chalcone IDNA-lipid as a function of  $R$ . See eq 9. <sup>f</sup> As evaluated from the evolution of the fluorescence intensity of the chalcone IDNA-lipid as a function of  $R$  in the presence of Rh-PE-containing vesicle. See eq 9.

coexistence of spherical micelles and vesicles was continuously observed. Using EM photographs from the titrating vesicle suspension and from the initial micellar solution of IGeB as references (respectively, Figure 1, panels a and b), we concluded that (i) IGeB did not promote any vesicle breakage; (ii) the concentration in micelles did not considerably drop during the titration until 2–3 mM of EPC were added. These observations led us to mainly interpret the process observed by steady-state emission of fluorescence in the sub-millimolar EPC concentration range as a scrambling of lipids among present micelles and vesicles. Such exchanges of lipids at constant morphologies have been already reported between vesicles.<sup>45</sup> Above  $[\text{EPC}] \approx 2\text{--}3$  mM, the concentration in micelles noticeably drops, and, at 20 mM, one essentially only distinguished vesicles on EM photographs (Figure 1c). The EM investigation thus suggested that the value of the equilibrium constant  $K_{\text{m} \rightarrow \text{v}}$  associated to the reaction:



was at room temperature in the 100 range (roughly the inverse of the EPC concentration where half the micelles had disappeared).

To obtain a better estimate of  $K_{\text{m} \rightarrow \text{v}}$  without possible interference associated with sample conditioning for electron microscopy, the titration of 10 nM IGeB by 9.3 mM EPC LUV was followed by FCS in 100 mM NaCl, 10 mM Tris-HCl pH 7 buffer at 293 K. The autocorrelation curves collected during the titration displayed a biphasic behavior that was more readily observed in log-log plots such as in Figure 5a. Under the assumption, supported by EM observations, of the coexistence of two different fluorescent species, micelles and vesicles, these curves were analyzed according to eq 11 to extract the two prefactors  $g_{\text{micelles}}$  and  $g_{\text{vesicles}}$  (see Experimental Section). The average concentration of chalcone-containing LUVs was then computed for each titration point and finally fitted according to eqs 14 and 15 (Figure 5b) to obtain 20 as an estimate for  $K_{\text{m} \rightarrow \text{v}}$  at 293 K, which is in line with the order of magnitude derived from EM observations.

The present series of experiments demonstrates that the mixture of IDNA and EPC is heterogeneous in a large interval of EPC concentration (0–2 mM) where vesicles and micelles coexist while essentially exchanging lipids. Larger concentrations of EPC are required to promote complete incorporation of IDNA within vesicle walls. This result is in marked contrast

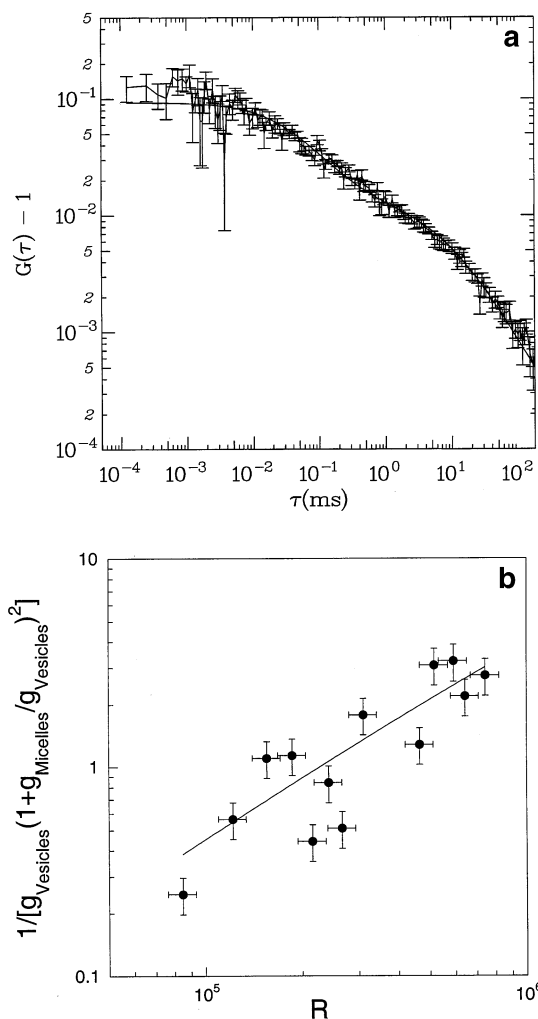


**Figure 5.** (a) Autocorrelation curve recorded at 293 K from a solution 10 nM in **IGeB** and 0.85 mM in EPC ( $\lambda_{\text{exc}} = 780$  nm) leading to  $\tau_{\text{Dmicelles}} = 38 \mu\text{s}$  and  $\tau_{\text{Dvesicles}} = 7.8$  ms; (b) Evolution of  $1/[g_{\text{vesicles}}(1 + (g_{\text{micelles}}/g_{\text{vesicles}})^2)]$  as a function of  $R = [\text{EPC}]_{\text{tot}}/[\text{IGeB}]_{\text{tot}}$  during the titration by FCS of 10 nM **IGeB** by 9.3 mM EPC vesicles in 100 mM NaCl, 10 mM Tris-HCl/Tris pH 7 buffer at 293 K. See text and Experimental Section.

with the one obtained for the largely favored transfer of the conjugate into OG micelles. In fact, anchoring ss-DNA at a bilayer surface has an entropic cost because of the polymer confinement in a half-space; meanwhile, changing the hydrophobic environment of the chalcone (from a micellar core to phospholipidic chains) does not necessarily lead to an important enthalpic gain. Comparatively, the transfer into the small ellipsoidal OG micelles<sup>38</sup> occurs at nearly constant surface curvature, whereas the micellar core becomes more hydrophobic due to the presence of numerous small detergent molecules.

Finally, we can notice that the insertion in LUVs is more difficult for chalcone conjugate than for cholesterol ones. From the literature<sup>18</sup> and on the basis of a simple 1:1 complexation model,<sup>44</sup> we could evaluate an underestimate equal to  $10^3$  for the partition coefficient of cholesterol-DNA between the solution and vesicles. The latter value is about hundred times larger than  $K_{m \rightarrow v}$ . Our interpretation for this difference of behavior relies on the less pronounced hydrophobicity of cholesterol with regard to the present chalcone moiety: cholesterol-DNA anchors more easily in bilayers because they do not form stable micelles in water.

**Pairing Properties of IDNAs.** The preceding paragraphs emphasized the significance of the hydrophobic tail in determin-

**TABLE 3: Melting Temperatures of the ds-DNA and ds-IDNA Duplexes as Measured from Denaturation Experiments Followed by Absorption at 260 nm or by BOBO3 Fluorescence<sup>a</sup>**

ds-DNA sequences	nonconjugated oligonucleotide	conjugated oligonucleotide <sup>c</sup>	
		without Triton X-100	with Triton X-100
G/C	53, 56 <sup>b</sup>		
GeB/C	54	51 (b)	50
GeB'/C	53	50 (b)	51
GeB/ACA	51	?	52 (b)
GeB'/A'CA'	51	?	50 (b)

<sup>a</sup> Buffer 100 mM NaCl, 10 mM  $\text{Na}(\text{CH}_3)_2\text{AsO}_2\text{-HCl}$  pH 7; concentrations of  $2 \mu\text{M}$  per strand). When present, Triton X-100 was at 0.36 mM concentration. See text and Experimental Section. <sup>b</sup> Measured by the assay relying on BOBO3<sup>®</sup> fluorescence. <sup>c</sup> (b) refers to a broad transition, ? denotes that it was impossible to determine the melting temperature during the corresponding experiment.

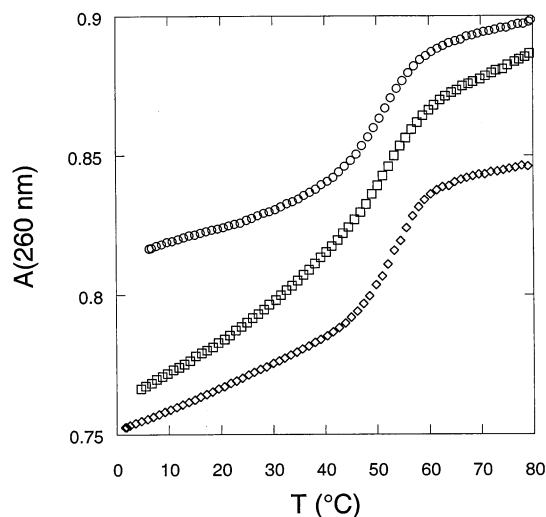


**Figure 6.** Experimental DNA denaturation curves from different experiments involving G/C pairing: **GeB'/C** (circles), **IGeB'/C** (squares), **IGeB'/C** + 0.36 mM Triton X-100 (diamonds).  $2 \mu\text{M}$  concentration for each DNA single strand. 100 mM NaCl, 10 mM  $\text{Na}(\text{CH}_3)_2\text{AsO}_2\text{-HCl}$  pH 7 buffer. To improve reading, a vertical offset was added.

ing self-aggregation that hindered incorporation of conjugates into vesicle bilayers. In relation with the initial goal and with potential use as antisense drug, we were also concerned with the possible interference of IDNA alkyl chains in the pairing process between complementary oligonucleotides. In fact, the lipid backbone was anticipated to interact with the nucleic bases either in the single or in the double-stranded DNA form.

We first measured the melting temperatures ( $T_m$ ) for different combinations of complementary strands (G/C, GeB/C, GeB'/C, GeB/ACA, GeB'/A'CA'). Either the absorbance at 260 nm or the fluorescence emission from the intercalating agent BOBO3 were recorded as a function of the temperature (See Experimental Section).  $T_m$  values ranging between 50 and 55 °C, associated to sharp transitions, were typically obtained (Table 3 and Table 1S). In contrast, when **IGeB** and **IGeB'** were used for pairing, we observed either broad transitions (**IGeB/C** and **IGeB'/C**) or no transition at all (**IGeB/ACA** and **IGeB'/A'CA'**; Figure 6). After addition of the detergent Triton X-100 above its CMC, the transitions arising from the same combinations of complementary strands became much more visible around 50–52 °C: sharp for **IGeB/C** and **IGeB'/C**, broad for **IGeB/ACA** and **IGeB'/A'CA'**.

Terminal lipophilic groups have variously been reported to decrease,<sup>15,17,21</sup> or have no effect at all<sup>16,21</sup> on stability of

oligonucleotide duplexes. The  $T_m$  variations were always small (less than 5 °C), and the present data are thus in line with previously published articles. However, the corresponding melting curves are scarce in the literature and we cannot evaluate whereas the broadening effect observed here is common.

In our experiment, the chalcone–DNA duplexes seem to start melting at a lower temperature than the nonconjugated ones. The denaturation curves cannot be fitted anymore by a simple all-or-none two-state model,<sup>46</sup> either because of a polydispersity effect or because of a more complex melting mechanism. Such observations demonstrate that the presence of the hydrophobic tail and the subsequent conjugate aggregation hinder at least partially hybridization between complementary strands. In fact, interaction between the alkyl chains and the nucleic bases is expected to decrease the affinity for pairing. Consequently, the recovery of the duplex melting properties when IDNA is mixed with Triton X-100 can be interpreted as follows: like when OG is present the lipophilic chains are buried into the micelle core; hence, they cannot interact anymore with the aromatic bases of DNA.

### Conclusion

Aiming to investigate the insertion of lipid-oligonucleotides into model bilayer, we synthesized conjugates labeled in their hydrophobic moiety by a solvatochromic chalcone. These derivatives were found to form micelles in aqueous solution with a critical micellar concentration lower than 10 nM. The implications related to the behavior of these DNA lipids were 2-fold. First, the gain in Gibbs free energy upon transferring the present DNA lipids from the pure micellar phase to the bilayer of small unilamellar vesicles was as low as a few  $k_B T$ . Partition between pure micelles and EPC vesicles was therefore not favorable except at the largest vesicle concentrations. Second, the aromatic nucleic bases probably interact with the aggregate lipophilic core and hybridization to complementary strands became less efficient with a decrease and a broadening of the melting transition.

The present results bear much significance for designing efficient strategies both for using bilayers scaffold to self-assembled lipids with large hydrophilic headgroups and for improving the activity of antisense medicines. Comparing these results to the ones reported for cholesterol conjugates (CMC above 100  $\mu$ M, insertion in bilayers favored and melting behavior nearly unchanged), we can indeed put forward that a too lipophilic group can be detrimental to the anchoring and the pairing properties of DNA lipids. In fact, such lipid moiety will not enhance the partition between the aqueous solution and the bilayer. In contrast, it will promote the formation of stable micelles impeding any further transfer to organized assemblies.

### Experimental Section

**Chemical Synthesis. General Procedures.** Microanalyses were performed by the Service de Microanalyses de l'Université Pierre et Marie Curie (Paris). Melting points were determined with a Büchi 510 capillary apparatus. <sup>1</sup>H and <sup>13</sup>C NMR spectra were recorded at room temperature on a Bruker AM 200 SY or an Avance Bruker DRX 400 spectrometer; chemical shifts are reported in ppm using the solvent as internal reference (<sup>1</sup>H, CHCl<sub>3</sub> in CDCl<sub>3</sub> 7.27 ppm; <sup>13</sup>C, <sup>13</sup>CDCl<sub>3</sub> in CDCl<sub>3</sub> 77.0 ppm); coupling constants  $J$  are given in Hz. Mass spectra (chemical ionization with NH<sub>3</sub> or FAB positive) were performed by the Service de Spectrométrie de Masse de l'ENS (Paris). Column chromatography was performed on silica gel 60 (0.040–0.063 mm) Merck. Analytical or preparative thin-layer chromatography (TLC) was conducted on Merck silica gel 60 F<sub>254</sub> precoated

plates. Commercially available reagents were used as obtained. Dry solvents were distilled according to classical procedures.

***N,N*-Dihexadecylaniline (3).** A suspension of freshly distilled aniline **1** (5 mL, 54 mmol, 1 equiv), 1-bromohexadecane **2** (50 mL, 162 mmol, 3 equiv), dry potassium carbonate (22.4 g, 162 mmol, 3 equiv) and dry potassium iodide (10.75 g, 65 mmol, 1.2 equiv), in dry *n*-butanol (100 mL) was vigorously stirred under nitrogen at 110 °C for 72 h. After cooling to room temperature, the mixture was filtered and the *n*-butanol was evaporated under vacuum. The residue was dissolved in ether (100 mL) and washed with distilled water (3 × 50 mL). The organic layer was dried over potassium carbonate and concentrated under reduced pressure. Recrystallization in absolute ethanol gave **3** as white crystals (25.0 g, 85% yield). <sup>1</sup>H NMR (CDCl<sub>3</sub>, 200 MHz,  $\delta$ , ppm): 7.24–7.16 (m, 3H), 6.63 (m, 2H,  $J$  = 8.0 Hz), 3.24 (t, 4H,  $J$  = 7.6 Hz), 1.60–1.20 (m, 56H), 0.89 (t, 6H,  $J$  = 6.4 Hz); <sup>13</sup>C NMR (CDCl<sub>3</sub>, 50 MHz,  $\delta$ , ppm): 148.0, 129.0, 114.9, 111.5, 50.9, 31.8, 29.5, 29.5, 29.5, 29.5, 29.4, 29.2, 27.1, 27.0, 22.5, 14.0; C<sub>38</sub>H<sub>71</sub>N (541.99): Anal. Calcd., C,84.21; H,13.20; N, 2.58; Found, C,83.93; H,13.63; N, 2.61.

**4-*N,N*-Dihexadecylaminobenzaldehyde (4).** Phosphoryl chloride (2 mL, 21.6 mmol, 1.2 equiv) was added to a solution of dry *N,N*-dimethylformamide (50 mL, 0.64 mol, 35 equiv) at 0 °C under nitrogen. The mixture was warmed to 50 °C for 10 min when a yellow–orange color appeared. A solution of **3** (9.75 g, 18 mmol, 1 equiv) in dry *N,N*-dimethylformamide (30 mL) was added and the mixture was warmed to 100 °C for 3 h. After cooling to room temperature, the mixture was quenched by adding water (50 mL), neutralized with a saturated aqueous solution of NaHCO<sub>3</sub> and extracted with cyclohexane (100 mL). The organic layer was washed with distilled water (3 × 50 mL), dried over potassium carbonate, and concentrated under reduced pressure. After recrystallization in absolute ethanol, white crystals of **4** were obtained (8.7 g, 85% yield). <sup>1</sup>H NMR (CDCl<sub>3</sub>, 200 MHz,  $\delta$ , ppm): 9.70 (s, 1H), 7.70 (d, 2H,  $J$  = 8.9 Hz), 6.64 (d, 2H,  $J$  = 8.9 Hz), 3.34 (t, 4H,  $J$  = 7.6 Hz), 1.60–1.20 (m, 56H), 0.89 (t, 6H,  $J$  = 6.4 Hz); <sup>13</sup>C NMR (CDCl<sub>3</sub>, 50 MHz,  $\delta$ , ppm): 189.8, 152.5, 132.0, 124.4, 110.6, 51.0, 31.9, 29.6, 29.6, 29.6, 29.5, 29.4, 29.3, 27.1, 27.0, 22.6, 14.1; C<sub>39</sub>H<sub>71</sub>NO (570.00): Anal. Calcd., C, 82.17; H, 12.55; N, 2.45; Found, C, 82.02; H, 12.57; N, 2.40.

**4-{2-[2-(2-Hydroxy-ethoxy)-ethoxy]-ethoxy}acetophenone (7).** A suspension of 4-hydroxyacetophenone **5** (3.9 g, 30 mmol, 1 equiv), 2-[2-(2-chloroethoxy)ethoxy]ethanol **6** (5.2 mL, 36 mmol, 1.2 equiv), dry potassium carbonate (6.2 g, 45 mmol, 1.5 equiv) and dry potassium iodide (6.5 g, 39 mmol, 1.3 equiv) in dry *n*-butanol (60 mL) was vigorously stirred under nitrogen at 110 °C for 12 h. After cooling to room temperature, the reaction mixture was filtered and the *n*-butanol was evaporated under vacuum. The residue was dissolved in dichloromethane (100 mL). The resulting organic solution was washed with sodium hydroxide 5% (50 mL) and with distilled water (3 × 50 mL). The organic layer was dried over potassium carbonate and concentrated under reduced pressure to give a pale yellow oil (7.7 g, 95% yield). <sup>1</sup>H NMR (CDCl<sub>3</sub>, 200 MHz,  $\delta$ , ppm): 7.92 (d, 2H,  $J$  = 8.9 Hz), 6.95 (d, 2H,  $J$  = 8.9 Hz), 4.20 (t, 2H,  $J$  = 4.3 Hz), 3.86 (t, 2H,  $J$  = 4.3 Hz), 3.80–3.55 (m, 8H), 2.52 (s, 3H); <sup>13</sup>C NMR (CDCl<sub>3</sub>, 50 MHz,  $\delta$ , ppm): 196.7, 162.4, 130.4, 130.3, 114.1, 72.3, 70.7, 70.1, 69.3, 67.3, 61.5, 26.2; C<sub>14</sub>H<sub>20</sub>O<sub>5</sub> (268.31): Anal. Calcd., C,62.67; H,7.51; Found, C,-62.59; H,7.65.

**4-*N,N*-Dihexadecylamino-4'-{2-[2-(2-Hydroxy-ethoxy)-ethoxy]-ethoxy}chalcone (8).** A solution of **4** (569 mg, 1 mmol, 1 equiv)

and **7** (268 mg, 1 mmol, 1 equiv) in absolute ethanol/dichloromethane: 1/1 (3 mL) was stirred at 35 °C. Solid potassium hydroxide was progressively added to the reaction flask: 280 mg (5 mmol, 5 equiv), then 280 mg (5 mmol, 5 equiv) after stirring for 2 h, and 840 mg (15 mmol, 15 equiv) 1 h later. After the sample was stirred for 36 h at 35 °C, the reaction mixture was cooled to room temperature and quenched by adding distilled water (100 mL) and dichloromethane (100 mL). The organic layer was washed with a saturated aqueous solution of NaCl, dried over sodium sulfate, and concentrated under reduced pressure. Purification by column chromatography (silica gel; ethyl acetate) yielded **8** as a yellow solid (154 mg, 63%). <sup>1</sup>H NMR (CDCl<sub>3</sub>, 200 MHz, δ, ppm): 8.01 (d, 2H, *J* = 8.8 Hz), 7.78 (d, 1H, 15.4 Hz), 7.52 (d, 2H, *J* = 8.8 Hz), 7.32 (d, 1H, *J* = 15.4 Hz), 6.98 (d, 2H, *J* = 8.8 Hz), 6.62 (d, 2H, *J* = 8.8 Hz), 4.21 (t, 2H, *J* = 4.6 Hz), 3.89 (t, 2H, *J* = 4.6 Hz), 3.80–3.55 (m, 8H), 3.31 (t, 4H, *J* = 7.3 Hz), 1.60–1.20 (m, 56H), 0.89 (t, 6H, *J* = 6.4 Hz); <sup>13</sup>C NMR (CDCl<sub>3</sub>, 50 MHz, δ, ppm): 188.8, 161.9, 149.8, 145.0, 132.1, 130.5, 130.4, 121.8, 115.8, 114.1, 111.2, 72.4, 70.8, 70.3, 69.5, 67.4, 61.7, 51.0, 31.8, 29.6, 29.6, 29.6, 29.5, 29.4, 29.3, 27.2, 27.0, 22.6, 14.0; C<sub>53</sub>H<sub>89</sub>NO<sub>5</sub> (820.30): Anal. Calcd., C, 77.61; H, 10.94; N, 1.71; Found, C, 77.43; H, 11.09; N, 1.58.

*4-N,N-Dihexadecylamino-4'-[2-[2-(2-Chloro-ethoxy)-ethoxy]-ethoxy]chalcone (9)*. A mixture of **4** (260 mg, 0.32 mmol, 1 equiv), triphenylphosphine (320 mg, 1.22 mmol, 3.8 equiv) and imidazole (83 mg, 1.22 mmol, 3.8 equiv) in carbon tetrachloride (5 mL) was stirred vigorously at reflux under nitrogen for 3 h. The mixture was cooled to room temperature, and the solvent was evaporated under vacuum. The residue was dissolved in ether (50 mL) and washed with water (3 × 50 mL). After the organic layer was dried over potassium carbonate and solvent was evaporated, the crude residue was purified by column chromatography (silica gel; cyclohexane/ethyl acetate 9/1) to yield **9** as an orange solid (210 mg, 80% yield). <sup>1</sup>H NMR (CDCl<sub>3</sub>, 200 MHz, δ, ppm): 8.01 (d, 2H, *J* = 8.8 Hz), 7.78 (d, 1H, *J* = 15.4 Hz), 7.52 (d, 2H, *J* = 8.8 Hz), 7.32 (d, 1H, *J* = 15.4 Hz), 6.98 (d, 2H, *J* = 8.8 Hz), 6.62 (d, 2H, *J* = 8.8 Hz), 4.21 (t, 2H, *J* = 4.5 Hz), 3.89 (t, 2H, *J* = 4.5 Hz), 3.80–3.55 (m, 8H), 3.31 (t, 4H, *J* = 7.3 Hz), 1.60–1.20 (m, 56H), 0.89 (t, 6H, *J* = 6.4 Hz); <sup>13</sup>C NMR (CDCl<sub>3</sub>, 50 MHz, δ, ppm): 188.7, 162.0, 149.8, 145.0, 132.1, 130.4, 130.3, 121.8, 115.8, 114.1, 111.2, 71.3, 70.8, 70.6, 69.6, 67.4, 51.0, 42.6, 31.8, 30.1, 29.6, 29.6, 29.6, 29.5, 29.4, 29.3, 27.2, 27.0, 22.6, 14.0; C<sub>53</sub>H<sub>88</sub>ClNO<sub>4</sub> (838.74): Anal. Calcd., C, 75.90; H, 10.57; N, 1.67; Found, C, 75.73; H, 10.64; N, 1.57.

*4-N,N-Dihexadecylamino-4'-[2-[2-(2-Iodo-ethoxy)-ethoxy]-ethoxy]chalcone (10)*. A suspension of **9** (226 mg, 0.27 mmol, 1 equiv) and sodium iodide (1.2 g, 8 mmol, 30 equiv) in 2-butanone (20 mL) freshly dried over aluminum oxide was stirred at reflux for 48 h. After the sample was cooled to room temperature and concentrated under reduced pressure, the residue was dissolved in dichloromethane (100 mL). The organic phase was washed with a saturated aqueous solution of sodium thiosulfate (2 × 50 mL) and with distilled water (2 × 50 mL). After the organic layer was dried over sodium sulfate and the solvent was evaporated, the crude residue was purified by column chromatography (silica gel; dichloromethane/absolute ethanol 97/3) to give **10** as a yellow solid (208 mg, 81%). <sup>1</sup>H NMR (CDCl<sub>3</sub>, 250 MHz, δ, ppm): 8.01 (d, 2H, *J* = 8.8 Hz), 7.78 (d, 1H, *J* = 15.4 Hz), 7.52 (d, 2H, *J* = 8.8 Hz), 7.32 (d, 1H, *J* = 15.4 Hz), 6.99 (d, 2H, *J* = 8.8 Hz), 6.62 (d, 2H, *J* = 8.8 Hz), 4.22 (t, 2H, *J* = 4.7 Hz), 3.91 (t, 2H, *J* = 4.7 Hz), 3.80–3.60 (m, 6H), 3.40–3.20 (m, 8H), 1.70–1.20 (m, 56H),

0.88 (t, 6H, *J* = 6.5 Hz); <sup>13</sup>C NMR (CDCl<sub>3</sub>, 100 MHz, δ, ppm): 188.8, 162.0, 149.9, 145.0, 132.1, 130.5, 130.4, 121.8, 115.8, 114.2, 111.2, 71.9, 70.8, 70.2, 69.6, 67.5, 51.0, 31.9, 29.6, 29.6, 29.5, 29.4, 29.3, 27.2, 27.0, 22.6, 14.1, 2.8; MS (CI, NH<sub>3</sub>); *m/z* 930.7 (calc. avg. mass for C<sub>53</sub>H<sub>88</sub>INO<sub>4</sub> + H: 931.2); C<sub>53</sub>H<sub>88</sub>INO<sub>4</sub> (930.18): Anal. Calcd., C, 68.44; H, 9.54; N, 1.51; Found, C, 68.39; H, 9.60; N, 1.43.

*4-N,N-Dihexadecylamino-4'-[2-[2-(2-Azido-ethoxy)-ethoxy]-ethoxy]chalcone (11)*. A solution of **9** (427 mg, 0.5 mmol, 1 equiv) and sodium azide (65 mg, 1 mmol, 2 equiv) in dry *N,N*-dimethylformamide (5 mL) was stirred at 80 °C for 12 h. After cooling to room temperature, the mixture was quenched with distilled water (20 mL) and extracted with ethyl ether (4 × 20 mL). The combined organic layers were washed with brine, dried over sodium sulfate, and concentrated under reduced pressure. After the residue was purified by column chromatography (silica gel; cyclohexane/ethyl acetate 85/15), **11** was obtained as a viscous oil (389 mg, 90% yield). <sup>1</sup>H NMR (CDCl<sub>3</sub>, 200 MHz, δ, ppm): 8.01 (d, 2H, *J* = 8.8 Hz), 7.78 (d, 1H, *J* = 15.4 Hz), 7.52 (d, 2H, *J* = 8.8 Hz), 7.32 (d, 1H, *J* = 15.4 Hz), 6.98 (d, 2H, *J* = 8.8 Hz), 6.62 (d, 2H, *J* = 8.8 Hz), 4.21 (t, 2H, *J* = 4.7 Hz), 3.90 (t, 2H, *J* = 4.7 Hz), 3.80–3.60 (m, 6H), 3.42–3.27 (m, 6H), 1.60–1.20 (m, 56H), 0.88 (t, 6H, *J* = 6.4 Hz); <sup>13</sup>C NMR (CDCl<sub>3</sub>, 50 MHz, δ, ppm): 188.7, 162.0, 149.8, 145.0, 132.0, 130.4, 130.3, 121.7, 115.8, 114.1, 111.2, 70.8, 70.6, 70.0, 69.6, 67.4, 50.9, 50.6, 31.8, 29.6, 29.6, 29.6, 29.5, 29.4, 29.3, 27.2, 27.0, 26.8, 22.6, 14.0; MS (FAB, MB); *m/z* 845.8 (calc. avg. mass for C<sub>53</sub>H<sub>88</sub>N<sub>4</sub>O<sub>4</sub>: 845.31).

*4-N,N-Dihexadecylamino-4'-[2-[2-(2-Amino-ethoxy)-ethoxy]-ethoxy]chalcone (12)*. A mixture of **11** (359 mg, 0.425 mmol, 1 equiv), triphenylphosphine (167 mg, 0.64 mmol, 1.5 equiv) and 2 drops of distilled water in tetrahydrofuran (15 mL) was stirred at room temperature for 24 h. The solution was dried over potassium carbonate and concentrated under reduced pressure. Purification of the residue by column chromatography (silica gel; chloroform/methanol/distilled water 15/5/0.5) as eluent gave **12** as a yellow solid (310 mg, 90%). <sup>1</sup>H NMR (CDCl<sub>3</sub>, 200 MHz, δ, ppm): 8.01 (d, 2H, *J* = 8.8 Hz), 7.78 (d, 1H, *J* = 15.4 Hz), 7.52 (d, 2H, *J* = 8.8 Hz), 7.32 (d, 1H, *J* = 15.4 Hz), 6.98 (d, 2H, *J* = 8.8 Hz), 6.62 (d, 2H, *J* = 8.8 Hz), 6.34 (brs, 2H, NH<sub>2</sub>), 4.21 (t, 2H, *J* = 4.4 Hz), 3.87 (t, 2H, *J* = 4.4 Hz), 3.75–3.60 (m, 6H), 3.34 (t, 4H, *J* = 7.3 Hz), 3.08 (t, 2H, CH<sub>2</sub>NH<sub>2</sub>), 1.60–1.20 (m, 56H), 0.88 (t, 6H, *J* = 6.4 Hz); <sup>13</sup>C NMR (CDCl<sub>3</sub>, 50 MHz, δ, ppm): 188.7, 161.8, 149.8, 145.1, 132.0, 130.5, 130.3, 121.7, 115.6, 114.2, 111.2, 70.5, 70.0, 69.3, 68.1, 67.3, 50.9, 39.9, 31.8, 29.6, 29.6, 29.5, 29.5, 29.4, 29.2, 27.2, 27.0, 22.6, 14.0; MS (CI, NH<sub>3</sub>); *m/z* 819.9 (calc. avg. mass for C<sub>53</sub>H<sub>90</sub>N<sub>2</sub>O<sub>4</sub>: 819.31).

**Synthesis of Derivatized Oligonucleotides. Coupling Reaction.** Commercially available reagents were used as obtained. Water is of Millipore 18 MΩcm<sup>-1</sup> quality. Triethylamine was distilled over acetic anhydride. The oligonucleotides were purchased from Eurogentec (Seraing, Belgium) and their 5' to 3' sequences can be summarized as follow: **A** = TCG TTC AAT TC; **A'** = GAA TTG AAC GA; **B** = ACA ATT CGA T; **B'** = ATC GAA TTG T; **C** = ACG CGT AGG ACC; **G** = GGT CCT ACG CGT; **e** designates a triethyleneglycol spacer.

The derivatization of the commercial oligonucleotides requires different standard protocols that are described in a paper of Grimm et al.<sup>29</sup> First, oligonucleotides with a terminal 5' phosphate group were precipitated by hexadecyltrimethylammonium bromide (CTAB), dissolved in dimethyl sulfoxide (DMSO) and activated by a triphenylphosphine/dipyridyl disulfide/dimethyl-aminopyridine mixture.

For attachment of amino-modified chalcone **12**, the solution of chromophore in DMSO (1 mg/50  $\mu\text{L}$ ) was directly added to activated oligonucleotide and incubated at least 2 h, preferably overnight. The yield of the conjugate was between 40 and 85%. Then the product was precipitated by ethanol/sodium acetate solution and purified on 1.5% agarose gel in the presence of 0.1% Triton X-100. Formation of micelles did not permit us to purify the conjugate on HPLC or by denaturing polyacrylamide gel electrophoresis, as it is normally done.<sup>29</sup>

For attachment of iodoalkyl derivative of the chalcone, a slightly longer procedure was used. The activated oligonucleotide was precipitated by  $\text{LiClO}_4$ /acetone solution, washed by acetone, and quickly dissolved in the water solution of cystamine (5 mg/50  $\mu\text{L}$ ) together with 5  $\mu\text{L}$  of triethylamine. After incubation of the sample at least for 2 h at room temperature, the derivative was precipitated by ethanol/sodium acetate, redissolved in water, and reduced by 0.1 M dithiothreitol to afford cysteamino-modified oligonucleotide phosphoroamidate with a terminal -SH group. After precipitation of the sample by CTAB, the dried derivative was dissolved in DMSO, alkylated by the iodoalkyl-chalcone **10** (10–100 fold molar excess) in the presence of triethylamine, reprecipitated by ethanol/acetate, and purified on 1.5% agarose gel in the presence of 0.1% Triton X-100. Yields were typically in the 10% range.

**Purification by Agarose Gel Electrophoresis.** The electrophoresis was performed with a 1.5% GTG NuSieve agarose gel (FMC, Rockland, ME; buffer 10 mM BisTris 1 mM EDTA pH 6.5). The band corresponding to the desired derivatized oligonucleotide was submitted to the action of  $\beta$ -agarase (New England Biolabs, Beverly, MA) according to manufacturer's recommendations. To remove remaining oligosaccharides, the derivate was again precipitated by CTAB, the supernatant was discarded, and the pellet was dissolved in methanol and centrifuged. Nonsoluble particles were discarded, and the dissolved derivate was precipitated by ethanol/sodium acetate. The final product was dissolved in water and stored at  $-20\text{ }^\circ\text{C}$ . The sample concentration was evaluated from the UV absorption spectrum using the following values of the molar absorption coefficients given by Eurogentec:  $\epsilon_{\text{GeB}}(260\text{ nm}) = 210\,600\text{ M}^{-1}\text{cm}^{-1}$ ;  $\epsilon_{\text{GeB}}(260\text{ nm}) = 209\,800\text{ M}^{-1}\text{cm}^{-1}$ . For IDNA originating from the conjugation of thiol-terminated oligonucleotides, the latter values made it possible to derive the molar absorption coefficient corresponding to the chalcone moiety. In 100 mM NaCl, 10 mM  $\text{Na}(\text{CH}_3)_2\text{AsO}_2\text{-HCl}$  pH 7 buffer, one obtained:  $\epsilon_{\text{IDNA}}(\lambda_{\text{max}} = 433\text{ nm}) = 24\,000\text{ M}^{-1}\text{cm}^{-1}$  and  $\epsilon_{\text{IDNA}}(\lambda_{\text{max}} = 433\text{ nm}) = 32\,000\text{ M}^{-1}\text{cm}^{-1}$ .<sup>47</sup>

**UV/Vis Absorption and Steady-State Emission Spectroscopies.** UV/Vis absorption spectra were recorded on a Uvikon-930 spectrophotometer (Kontron, Zürich, Switzerland). Corrected fluorescence spectra and excitation polarization spectra were obtained with a LPS 220 spectrofluorometer (PTI, Monmouth Junction, NJ). Steady-state fluorescence anisotropies defined as  $\langle r \rangle = (I_{\parallel} - I_{\perp}) / (I_{\parallel} + 2I_{\perp})$  were determined by the G-factor method ( $I_{\parallel}$ , respectively  $I_{\perp}$ , being the fluorescence intensity observed with vertically polarized excitation light and vertically, respectively horizontally, polarized emissions).<sup>48</sup> The temperature was regulated at  $0.1\text{ }^\circ\text{C}$  and directly measured within the cuvettes.

**Electron Microscopy (EM).** Samples containing EPC vesicles were prepared by dialysis. After staining of the samples with 2% uranyl acetate, they were observed on a Philips CM208 transmission electron microscope operating at 80 kV. Electron micrographs were recorded at a nominal magnification of 40 000.

**Fluorescence Correlation Spectroscopy (FCS) Measurements.** *FCS Setup.* The two-photon excitation FCS setup consists of a laser source, a home-built microscope, and two avalanche photodiodes (ADP; see Supporting Information, Figure 3S). The laser source is a mode-locked Ti:Sapphire laser (Mira 900, Coherent, Auburn, CA) pumped by a solid-state laser at 532 nm (Verdi, Coherent). Pumped at 5 W, the Ti:Sapphire laser generates 200 fs pulses at 80 MHz with about 700 mW average power output at 800 nm. The whole tunable spectral range covers the 700–1000 nm region. The power is adjusted by means of neutral filters. The laser beam is expanded 3 times at the entrance of the microscope in order to reach a diameter of approximately 7 mm to fill up the back entrance of the employed objective. After the beam expander, the light is passed through a dichroic mirror and focused into the sample with a  $60\times$  water-immersion objective (NA = 1.2, UPlanApo, Olympus). The sample is contained within a 1-mm square glass capillary (VitroCom, Mountain Lakes, NJ). The fluorescence is collected through the same objective, reflected by the dichroic mirror and filtered through four short pass filters to absorb any possible diffused infrared light. The light is then separated by a cube beam-splitter with a 1:1 ratio and focused on the 200  $\mu\text{m}^2$  working surfaces of two APDs (SPCM-AQR-14, Perkin-Elmer, Vaudreuil, Canada). The signal output of the APDs modules (TTL pulses) are acquired by a digital autocorrelator module (ALV-6000, ALV, Langen, Germany) which computes on-line the cross-correlation function of the fluorescence fluctuations. Using two APDs and cross-correlation function reduces significantly the afterpulsing noise that is strongly correlated in the range shorter than 10  $\mu\text{s}$ . The resulting function is formally similar to the autocorrelation function. The data are then stored in the computer and analyzed by a home-written routine which allows us to (i) average chosen successive acquisitions; (ii) make a least-squares fit for both single- and two-components cross-correlation functions with diffusion in two- or three-dimensions; (iii) calculate the associated standard deviations.

*Calibration of the FCS Setup.* The fluctuations of fluorescence intensity  $I$  from a volume  $V$  containing freely diffusing fluorescent molecules (average concentration  $\bar{C}$ ) were analyzed with the correlation function  $G(\tau)$  given by:

$$G(\tau) - 1 = \frac{\langle \delta I(t) \delta I(t + \tau) \rangle}{\langle I \rangle^2} = \frac{1}{CV} \frac{1}{\left(1 + \frac{\tau}{\tau_D}\right)} \frac{1}{\left(1 + \left(\frac{w_{xy}}{w_z}\right)^2 \frac{\tau}{\tau_D}\right)^{1/2}} \quad (6)$$

where  $\tau_D$  is the diffusion time through a 3D Gaussian excitation profile characterized by  $I_{\text{ex}} = I_0 \exp[-2(x^2 + y^2)/w_{xy}^2 - 2z^2/w_z^2]$ . In the case of two-photon excitation,

$$\tau_D = w_{xy}^2 / 8D \quad (7)$$

where  $D$  is the diffusion coefficient of the fluorescent species. Consequently, fitting the  $G(\tau) - 1$  curve for species of known diffusion coefficient allows us to calibrate the beam-waists  $w_{xy}$  and  $w_z$  of our experimental setup. Fluorescein labeled beads of 0.02  $\mu\text{m}$  radius  $R_H$  (Molecular Probes, Eugene, OR) were used under the assumption that

$$D = k_B T / 6\pi\eta R_H \quad (8)$$

(with  $k_B$  the Boltzmann constant,  $T$  the absolute temperature, and  $\eta$  the solvent viscosity); we found  $w_{xy} \approx 0.3\text{ }\mu\text{m}$  and  $(w_{xy}/$

$w_{xy}^2 \approx 0.01$ . The  $w_{xy}$  value corresponds to the expected one for the objective used ( $w_{xy} = 0.61\lambda_{\text{ex}}/\text{NA} \approx 0.4 \mu\text{m}$ ) and the excitation volume can be then calculated as  $V = \pi w_{xy}^4/\lambda_{\text{ex}}$ ,<sup>49</sup> typically in the femtoliter range.

**Power-Squared Dependence of Two-Photon-Excited Fluorescence.** The molecules under study were excited through the two-photon absorption process at  $\lambda_{\text{exc}} = 780 \text{ nm}$ . For FCS applications, it is essential to be in a regime in which the concentration of excited molecules is proportional to the square of the excitation power; otherwise, eqs 6 and 11 cannot be used for treating experimental data.<sup>50</sup> We investigated the dependence of the fluorescence as a function of the excitation power for all the compounds studied, and we chose the power such as to remain in the regime of power-squared dependence (see for instance Supporting Information, Figure 4S; as a rule, the power before the entrance of the beam expander was set less than 60 mW). With those experimental conditions, no contribution of the triplet state to the experimental FCS curves was observed either.

**Calibration of Medium Viscosity during Titrations by Micelles and Vesicles.** The diffusion time of fluorescent species extracted from FCS depends on solution viscosity (see eqs 7 and 8). Thus, to interpret the diffusion times only in terms of structural changes occurring during the subsequent titrations, it is necessary to calibrate medium viscosity as a function of the concentrations both in OG and in EPC vesicles to perform the relevant corrections. By recording, in a series of independent experiments, the  $G(\tau)$  curves originating from 10 nM fluorescein solutions in 100 mM NaCl, 10 mM Tris-HCl/Tris pH 9 buffer, we evaluated the variation of medium viscosity as a function of the concentrations in OG or in EPC vesicles. In the course of the corresponding studies, the experimental  $G(\tau)$  curves were satisfactorily fitted by eq 6, suggesting no significant interaction to arise between fluorescein and the organized media. We also observed that  $G(0)$  decreased and  $\tau_D$  increased during the titration by micelles or by concentrated vesicles. We checked that the corresponding observation was not related to changes of refractive index: titrating a 10 nM fluorescein solution in 100 mM NaCl, 10 mM Tris-HCl/Tris pH 9 buffer with concentrated sucrose led to the expected observations of no change in  $G(0)$  and an increase in  $\tau_D$  linked to viscosity. Therefore, we assume light diffusion by micelles and vesicles to expand the excitation profile without strongly altering its geometry, leading to the subsequent decrease in  $G(0)$ . Consequently, the calibration of viscosity was performed from  $\tau_D \sqrt{G(0)-1}$  instead of  $\tau_D$ : both functions are linearly dependent on viscosity, but the latter is also proportional to  $w_{xy}^2$  (from eqs 7 and 8), whereas the former does not depend on  $w_{xy}$  (from eqs 6–8 with  $V = \pi w_{xy}^4/\lambda_{\text{exc}}$ ). The reported value of viscosity for 100 mM NaCl at 293 K was used for determining the proportionality factor linking  $\eta$  to  $\tau_D \sqrt{G(0)-1}$ , yielding to the curves displayed in Supporting Information, Figure 5Sa,b. One notices that the viscosity of the OG solutions strongly increases above OG CMC (Supporting Information, Figure 5Sa), whereas the viscosity of suspensions of EPC vesicles remains essentially unaltered in the investigated range of EPC concentrations (Supporting Information, Figure 5Sb).

**Large Unilamellar Vesicles (LUVs) Preparation.** A solution containing  $\alpha$ -L-phosphatidylcholine (100 mg  $\text{mL}^{-1}$  in hexane; 50  $\mu\text{L}$ , 5 mg, 7  $\mu\text{mol}$ ), and 1-octyl- $\beta$ -D-glucopyranoside (10.4 mg; 36  $\mu\text{mol}$ , 5 equiv) in chloroform (0.5 mL) was evaporated to dryness under reduced pressure at room temperature. The film was then dissolved after addition of the suitable buffer (2 mL).

**Preparation by the Dialytic Detergent Removal Technique.**<sup>51</sup> The resulting solution was transferred to dialysis tubing (Viskase, MW cut off 12000–14000). Detergent was removed by dialysis at room temperature; typically 2 mL of detergent/lipid solution was dialyzed against 1 L of buffer solution and the dialysis solution was changed three times over 2 days.

**Preparation Relying on Detergent Removal with Bio-Beads.**<sup>52</sup> The suspension resulting from addition of buffer (2 mL) and previously conditioned<sup>53</sup> Bio-Beads SM2 (BioRad; 30 mg) was vortexed at room temperature for 2 h. Fresh Bio-Beads SM2 (60 mg) were added and the mixture was vortexed again for 1 h. This operation was repeated once with 30 mg of beads. The resulting vesicular suspension was filtered and immediately used. In the case of RhPE-containing vesicles, Rh-PE (Molecular Probes) was added together with EPC before chloroform evaporation.

**Determination of IDNA:EPC Association Constants.** The simple two-state models eqs 4 and 5 were introduced to describe the association between the IDNA and EPC LUV.<sup>44</sup> In these equations, the IDNA is assumed to give a 1:1 “complex” with an EPC molecule. The corresponding association constants ( $K_{\text{mix}}$  and  $K_{\text{m} \rightarrow \text{v}}$ ) were evaluated either by steady-state emission of fluorescence, electron microscopy, or fluorescence correlation spectroscopy.

**Evaluation by Steady-State Emission of Fluorescence.** In a first step, the fluorescence data were corrected from the dilution arising from vesicle addition. They were subsequently analyzed from the easily derived eq 9:<sup>54</sup>

$$I_{\text{F}}([\text{EPC}]) = I_{\text{F}}(0) - \frac{I_{\text{F}}(0) - I_{\text{F}}(\infty)}{2} \left\{ \left( 1 + R + \frac{1}{K_{\text{mix}}[\text{IDNA}]_{\text{tot}}} \right) - \left[ \left( 1 + R + \frac{1}{K_{\text{mix}}[\text{IDNA}]_{\text{tot}}} \right)^2 - 4R \right]^{1/2} \right\} \quad (9)$$

where  $I_{\text{F}}(0)$  and  $I_{\text{F}}(\infty)$  are the initial fluorescence intensity and the asymptotic limit of the fluorescence intensity at large EPC concentrations,  $[\text{IDNA}]_{\text{tot}}$  is the total concentration of IDNA during the titration,<sup>55</sup> and  $R$  is the ratio  $[\text{EPC}]_{\text{tot}}/[\text{IDNA}]_{\text{tot}}$  with  $[\text{EPC}]_{\text{tot}}$  referring to the total EPC concentration. The fit of the experimental data according to eq 9 provides orders of magnitude for  $I_{\text{F}}(\infty)/I_{\text{F}}(0)$  and for  $K_{\text{mix}}$ . Then, numerical calculations were further performed to refine the latter values:  $I_{\text{F}}([\text{EPC}])$  values were calculated from different  $\{I_{\text{F}}(\infty)/I_{\text{F}}(0), K_{\text{mix}}\}$  sets closely located around the previously derived orders of magnitude, and the final selected set was the one that gave the best simulation of the experimental data.

**Evaluation by Electron Microscopy.** In the concentration regime used for this series of experiments in which  $[\text{EPC}]_{\text{tot}}$  always exceeds  $[\text{IDNA}]_{\text{tot}}$ , one has:

$$[\text{IDNA}] = \frac{[\text{IDNA}]_{\text{tot}}}{1 + K_{\text{m} \rightarrow \text{v}}[\text{EPC}]_{\text{tot}}} \quad (10)$$

In particular,  $K_{\text{m} \rightarrow \text{v}}[\text{EPC}]_{\text{tot}} = 1$  for  $[\text{IDNA}] = [\text{IDNA}]_{\text{tot}}/2$ . The titration of 2.5  $\mu\text{M}$  IGeB by EPC vesicles in 100 mM NaCl, 10 mM  $\text{Na}(\text{CH}_3)_2\text{AsO}_2$ -HCl pH 7 buffer was performed up to  $[\text{EPC}]_{\text{tot}} = 20 \text{ mM}$ . The association constant was crudely evaluated as  $1/[\text{EPC}]_{\text{tot}}$  when half the initial IGeB micelles had disappeared from the EM picture.

**Evaluation by FCS.** The evaluation relies on the determination of the molar fractions of fluorescent IDNA in vesicles as a function of the total EPC concentration. Such amounts can be extracted from experiments devoted to measure diffusion coefficients since vesicles and micelles significantly differ in size.

In a regime of slow exchange of IDNA between the micelles and the vesicles, the correlation function of fluorescence intensity  $G(\tau)$  can be satisfactorily analyzed by eq 11, which accounts for two different species crossing a 2D-Gaussian excitation beam:<sup>56</sup>

$$G(\tau) - 1 = g_{\text{micelles}} \left(1 + \frac{\tau}{\tau_{D_{\text{micelles}}}}\right)^{-1} + g_{\text{vesicles}} \left(1 + \frac{\tau}{\tau_{D_{\text{vesicles}}}}\right)^{-1} \quad (11)$$

with

$$g_{\text{micelles}} = \frac{Q_{\text{micelles}}^2 \bar{N}_{\text{micelles}}}{(Q_{\text{micelles}}^2 \bar{N}_{\text{micelles}} + Q_{\text{vesicles}}^2 \bar{N}_{\text{vesicles}})^2} \quad (12)$$

and

$$g_{\text{vesicles}} = \frac{Q_{\text{vesicles}}^2 \bar{N}_{\text{vesicles}}}{(Q_{\text{micelles}}^2 \bar{N}_{\text{micelles}} + Q_{\text{vesicles}}^2 \bar{N}_{\text{vesicles}})^2} \quad (13)$$

In the above equations,  $\tau_{D_{\text{micelles}}}$  and  $\tau_{D_{\text{vesicles}}}$  are the characteristic diffusion times for crossing the excitation volume respectively associated with micelles and vesicles,  $\bar{N}_{\text{micelles}}$  and  $\bar{N}_{\text{vesicles}}$  the respective average numbers of labeled particles contained within the excitation volume  $V$ ,  $Q_{\text{micelles}}$ , and  $Q_{\text{vesicles}}$  the respective particles fluorescent brightness.

Both diffusion times were first measured independently.  $\tau_{D_{\text{micelles}}}$  was obtained from analyzing the correlation function  $G(\tau)$  arising from a 10 nM IGeB solution in 100 mM NaCl, 10 mM Tris-HCl/Tris pH 7 buffer according to eq 6.  $\tau_{D_{\text{vesicles}}}$  was similarly obtained from analyzing the correlation function  $G(\tau)$  arising from a vesicular suspension labeled with **8** ( $[\mathbf{8}] = 10$  nM) in 100 mM NaCl, 10 mM Tris-HCl/Tris pH 7 buffer. 50  $\mu\text{s}$  and 10 ms were typically found for  $\tau_{D_{\text{micelles}}}$  and  $\tau_{D_{\text{vesicles}}}$  respectively. We already demonstrated that medium viscosity did not change significantly upon vesicles additions and that the sizes of micelles and vesicles remained constant during all the titration (see EM); consequently,  $\tau_{D_{\text{micelles}}}$  and  $\tau_{D_{\text{vesicles}}}$  were anticipated to remain in the same order of magnitude whatever the amount of LUVs introduced.

The titration of a 10 nM IGeB solution by 9.3 mM EPC vesicles in 100 mM NaCl, 10 mM Tris-HCl/Tris pH 7 buffer was then performed. We checked that the extracted  $\tau_{D_{\text{micelles}}}$  and  $\tau_{D_{\text{vesicles}}}$  values for each EPC concentration were in the range determined during the first series of experiments, confirming that the morphology of the two phases, micelles and vesicles, remained essentially the same during the whole titration. Therefore, the process (5) and eq 10 were considered to satisfactorily model the phenomena during the whole titration. Then one can easily derive from eq 11 and conservation laws the following equations that allows for extracting  $K_{m \rightarrow v}$ :

$$\frac{1}{g_{\text{vesicles}}} = \bar{N}_{\text{vesicles}} Q_{\text{vesicles}}^2 \left(1 + \frac{g_{\text{micelles}}}{g_{\text{vesicles}}}\right)^2 \quad (14)$$

$$\bar{N}_{\text{vesicles}} = \frac{[\text{IDNA}]_{\text{tot}} V}{2} \left[ \left(1 + R + \frac{1}{K_{m \rightarrow v} [\text{IDNA}]_{\text{tot}}}\right) - \sqrt{\left(1 + R + \frac{1}{K_{m \rightarrow v} [\text{IDNA}]_{\text{tot}}}\right)^2 - 4R} \right] \quad (15)$$

Note that here we assumed vesicles bear a single fluorescent IDNA in view of the huge excess in LUVs.  $g_{\text{micelles}}$  and  $g_{\text{vesicles}}$  were first obtained from the fits of the experimental autocorrelation curves ( $\tau_{D_{\text{micelles}}}$  and  $\tau_{D_{\text{vesicles}}}$  having their values set to the ones resulting from the above independent measurements).

Then, the  $1/[g_{\text{vesicles}}(1 + (g_{\text{micelles}}/g_{\text{vesicles}}))^2]$  curve was plotted as a function of  $R$  and fitted according to eq 15 leaving the prefactor  $[\text{IDNA}]_{\text{tot}} V/2Q_{\text{vesicles}}^2$  and  $K_{m \rightarrow v}$  as floating parameters. Error on  $K_{m \rightarrow v}$  is evaluated to be 50%.

**DNA Melting Curves.** The 100 mM NaCl, 10 mM  $\text{Na}(\text{CH}_3)_2\text{AsO}_2\text{-HCl}$  pH 7 buffer was chosen for the low dependence of its pH with temperature.<sup>57</sup>

**Assay Relying on UV Absorption.** The experiments were performed with an UVikon spectrophotometer using the Macrotm software. Except for the samples containing micelles where the heating cycle was first applied, the absorbance at 260 nm was first recorded during a cooling cycle from 84 to 4 °C (0.1–0.2 °C min<sup>-1</sup>) and then during a heating cycle from 4 to 84 °C (0.1–0.2 °C min<sup>-1</sup>). No hysteresis was ever detected, suggesting that equilibrium is reached at each temperature. Half-dissociation temperatures ( $T_m$ ) were determined from the denaturation curves with a precision equal to 1 °C.<sup>46</sup>

**Assay Relying on Emission from an Intercalating Agent.** We designed this assay to measure the melting temperature of ds-DNA in vesicle suspensions. Indeed, the traditional method relying on recording the absorbance of DNA at 260 nm was not appropriate in a scattering medium where the extinction signal originating from particles strongly overcame the DNA absorption. The fluorescence emission of the intercalant BOBO3 (Molecular Probes) is strongly enhanced in the presence of ds-DNA and remains essentially unaffected in the presence of ss-DNA. Figure 6Sa (Supporting Information) displays, as a function of temperature, the collection of BOBO3 emission spectra (0.67  $\mu\text{M}$ ) in 100 mM NaCl, 10 mM  $\text{Na}(\text{CH}_3)_2\text{AsO}_2\text{-HCl}$  pH 7 buffer in the presence of C/G (2  $\mu\text{M}$ ). As anticipated, the emission drops when the temperature is increased. More precisely, the plot of BOBO3 emission ( $\lambda_{\text{exc}} = 530$  nm,  $\lambda_{\text{em}} = 600$  nm) as a function of temperature exhibits two different trends (Supporting Information; Figure 6Sb). First, the emission exhibits a smooth decrease over the whole temperature range as expected from the contribution of nonradiative desexcitation pathways of fluorescent probes that increases with the temperature. Second, emission suddenly drops between 40 and 65 °C,<sup>58</sup> generating a transition whose width is larger than the one observed during the classical assay. Inflection occurs at 56 °C, which compares satisfactorily with the 53 °C melting temperature measured by UV absorption. The apparent upward shift suggests that BOBO3 intercalation weakly stabilizes ds-DNA. Similar results were obtained in the presence of EPC vesicles, despite a smoother continuous decrease of fluorescence emission may be due to a direct interaction between BOBO3 and bilayers.

**Acknowledgment.** We are indebted to D. Bensimon who encouraged us to design 2D polymers relying on polycondensation between oligonucleotides. We also thank O. Ruel and J.-B. Baudin for advice concerning organic synthesis, L. Lacroix and J.-L. Mergny for introducing us to melting experiments, and T. Garestier and C. Hélène for helpful discussions.

**Supporting Information Available:** This material is available free of charge via the Internet at <http://pubs.acs.org>.

## References and Notes

- (1) (a) Seeman, N. *Acc. Chem. Res.* **1997**, *30*, 357–363. (b) Winfree, E.; Liu, F.; Wenzler, L.; Seeman, N. *Nature* **1998**, *394*, 539–544.
- (2) (a) Elgsaeter, A.; Stokke, B.; Mikklesen, A.; Branton, D. *Science* **1986**, *234*, 1217–1223. (b) Byers, T.; Branton, D. *Proc. Natl. Acad. Sci. U.S.A.* **1985**, *82*, 6153–6157. (c) Liu, S.-C.; Derick, L.; Palek, J. *J. Cell. Biol.* **1987**, *104*, 527–536.
- (3) (a) Kantor, Y.; Nelson, D. R. *Phys. Rev. Lett.* **1987**, *58*, 2774–2777. (b) Paczuski, M.; Kardar, M.; Nelson, D. R. *Phys. Rev. Lett.* **1988**,

- 60, 2638–2640. (c) Abraham, F. F.; Rudge, W. E.; Plischke, M. *Phys. Rev. Lett.* **1989**, *62*, 1757–1759. (d) Gompper, G.; Kroll, D. M. *Curr. Opin. Colloid Surface Sci.* **1997**, *2*, 373–381.
- (4) (a) Wen, X.; Garland, C. W.; Hwa, T.; Kadar, M.; Kokufuta, E.; Li, Y.; Orkisz, M.; Tanaka, T. *Nature* **1992**, *355*, 426–428. (b) Spector, M. S.; Naranjo, E.; Chiruvolu, S.; Zasadzinski, J. A. *Phys. Rev. Lett.* **1994**, *73*, 2867–2870. (c) Schmidt, C. F.; Svoboda, K.; Lei, N.; Petsche, I. B.; Berman, L. E.; Safinya, C. R.; Grest, G. S. *Science* **1993**, *259*, 952–955.
- (5) (a) Pearce, B.; Robison, M. *Annu. Rev. Cell. Biol.* **1990**, *6*, 151–171. (b) Marsh, M.; McMahon, H. *Science* **1999**, *285*, 215–220.
- (6) Alberts, B.; Bray, D.; Lewis, J.; Raff, M.; Roberts, K.; Watson, J. *Molecular Biology of the Cell*; Garland: New York, 1994.
- (7) Ringsdorf, H.; Schlarb, B.; Venzmer, J. *Angew. Chem., Int. Ed. Engl.* **1988**, *27*, 113–158.
- (8) Dubault, A.; Casagrande, C.; Veysssié, M. *J. Phys. Chem.* **1975**, *79*, 2254–2259.
- (9) (a) Miyano, K.; Veysssié, M. *Phys. Rev. Lett.* **1984**, *52*, 1318–1320. (b) Rehage, H.; Veysssié, M. *Angew. Chem., Int. Ed. Engl.* **1990**, *29*, 439–448.
- (10) (a) Gros, L.; Ringsdorf, H.; Schupp, H. *Angew. Chem., Int. Ed. Engl.* **1981**, *20*, 305–325. (b) Fendler, J. *Science* **1984**, *223*, 888–894. (c) Dvolaitzky, M.; Guedeau-Boudeville, M.-A.; Léger, L. *Langmuir* **1992**, *8*, 2595–2597. (d) O'Brien, D. F.; Armitage, B.; Benedicto, A.; Bennett, D. E.; Lamparshi, H. G.; Lee, Y.-S.; Srisiri, W.; Sisson, T. M. *Acc. Chem. Res.* **1998**, *31*, 861–868.
- (11) (a) Fukuda, H.; Diem, T.; Stefely, J.; Kezdy, F. J.; Regen, S. L. *J. Am. Chem. Soc.* **1986**, *108*, 2321–2327. (b) Ringsdorf, H.; Schlarb, B.; Tyminski, P. N.; O'Brien, D. F. *Macromolecules* **1988**, *21*, 671–677. (c) Higashi, N.; Adachi, T.; Niwa, M. *Macromolecules* **1990**, *23*, 1475–1480. (d) Lefevre, D.; Porteu, F.; Balog, P.; Roulliy, M.; Zalczet, G.; Palacin, S. *Langmuir* **1993**, *9*, 150–161. (e) Asakuma, S.; Okada, H.; Kunitake, T. *J. Am. Chem. Soc.* **1991**, *113*, 1749–1755.
- (12) Stupp, S.; Son, S.; Li, L.; Lin, H.; Keser, M. *J. Am. Chem. Soc.* **1995**, *117*, 5212–5227.
- (13) Boutorin, A. S.; Gus'kova, L. V.; Ivanova, E. M.; Kobetz, N. D.; Zarytova, V. F.; Ryte, A. S.; Yurchenko, L. V.; Vlassov, V. V. *FEBS Lett.* **1989**, *254*, 129–132.
- (14) Krieg, A. M.; Tonkinson, J.; Matson, S.; Zhao, Q.; Saxon, M.; Zhang, L.-M.; Bhanja, U.; Yakubov, L.; Stein, C. A. *Proc. Natl. Acad. Sci. U.S.A.* **1993**, *90*, 1048–1052.
- (15) Shea, R. G.; Marsters, J. C.; Bischofberger, N. *Nucleic Acids Res.* **1990**, *18*, 3777–3783.
- (16) (a) MacKellar, C.; Graham, D.; Will, D. W.; Burgess, S.; Brown, T. *Nucleic Acids Res.* **1992**, *20*, 3411–3417. (b) Manoharan, M.; Tivel, K. L.; Cook, P. D. *Tetrahedron Lett.* **1995**, *36*, 3651–3654.
- (17) Letsinger, R. L.; Alul, R. A.; Farooqui, F.; Gryaznov, S. M.; Kinstler, O. *Nucleic Acids Res.* **1991**, *Symp. Ser.* *24*, 75–78.
- (18) Bichenkov, E. E.; Budker, V. G.; Zarytova, V. F.; Ivanova, E. M.; Likhov, S. G.; Savchenko, E. V.; Teplova, N. M. *Biol. Membr.* **1988**, *5*, 735–742.
- (19) Tomkins, J. M.; Barnes, K. J.; Blaker, A. J.; Watkins, W. J.; Abell, C. *Tetrahedron Lett.* **1997**, *38*, 691–694.
- (20) Boutorin, A. S.; Tokuyama, H.; Takasugi, M.; Isobe, H.; Makamura, E.; Hélène, C. *Angew. Chem., Int. Ed. Engl.* **1994**, *33*, 2462–2465.
- (21) (a) Letsinger, R. L.; Zhang, G.; Sun, D. K.; Ikeuchi, T.; Sarin, P. S. *Proc. Natl. Acad. Sci. U.S.A.* **1989**, *86*, 6553–6556. (b) Stein, C. A.; Pal, R.; DeVico, A. L.; Hoke, G.; Mumbauer, S.; Kinstler, O.; Sarngadharan, M. G.; Letsinger, R. L. *Biochemistry* **1991**, *30*, 2439–2444.
- (22) Cheng, T. R.; Huang, C. H.; Gan, L. B.; Luo, C. P.; Yu, A. C.; Zhao, X. S. *J. Mater. Chem.* **1998**, *8*, 931–935.
- (23) (a) Lupo, D.; Prass, W.; Scheunemann, U.; Laschewsky, A.; Ringsdorf, H.; Ledoux, I. J. *Opt. Soc. Am. B* **1988**, *5*, 300–308. (b) Jones, G.; Stanforth, S. *Org. React.* **1997**, *49*, 1–330.
- (24) Pfeiffer, P. *Ann. Chem.* **1925**, *441*, 228–265.
- (25) (a) Nägeli, H.; Tambor, J. *Helv. Chem. Acta* **1924**, *7*, 333–336. (b) McLean, I.; Widdows, S. *J. Chem. Soc.* **1914**, *105*, 2169–2175.
- (26) Nakaya, K.; Funabiki, K.; Shibata, K.; Muramatsu, H.; Matsui, M. *Bull. Chem. Soc. Jpn.* **1996**, *69*, 2961–2966.
- (27) Matsui, M.; Oji, A.; Hiramatsu, K.; Shibata, K.; Muramatsu, H. *J. Chem. Soc., Perkin Trans. 2* **1992**, *2*, 201–206.
- (28) (a) Appel, R. *Angew. Chem., Int. Ed. Engl.* **1975**, *14*, 801–811. (b) Garreg, P.; Samulsson, B. *J. Chem. Soc., Perkin Trans. 1* **1980**, 2866–2869.
- (29) Grimm, G. N.; Boutorin, A. S.; Hélène, C. *Nucleos. Nucleot. Nucleic Acids* **2000**, *19*, 1943–1965.
- (30) Reichardt, C. *Solvents and Solvent Effects in Organic Chemistry*; VCH Publishers: Cambridge, 1988.
- (31) (a) Nikitina, A.; Fedyunina, G.; Umirzakov, B.; Yanovskaya, L.; Kucherov, V.; *Opt. Spectrosc.* **1973**, *34*, 163–165. (b) Katzenellenbogen, E.; Branch, G.; *J. Am. Chem. Soc.* **1947**, *69*, 1615–1619. (c) Gustav, K.; Bartsch, U.; Karnitzschky, K. *Z. Chem.* **1989**, *29*, 213–214. (d) Lavrishin, V.; Dzyuba, V.; Tolmachev, V. *J. Gen. Chem. USSR* **1966**, *36*, 1385–1389. (e) Tolochko, A.; Shevchuk, M.; Dombrovskii, A. *J. Org. Chem. USSR* **1972**, *8*, 2443–2447. (f) Yanorskaya, L.; Umirzakov, B.; Kucherov, V.; Yakovlev, I.; Zolotarev, B.; Chizhov, O.; Vorontsova, L.; Fundyler, I. *Tetrahedron* **1973**, *29*, 4321–4329. (g) Cromwell, N.; Watson, W. *J. Org. Chem.* **1949**, *14*, 411–420.
- (32) Valeur, B. *Molecular Fluorescence Principles and Applications*; Wiley-VCH: Weinheim, 2002.
- (33) Gosse, C.; Boutorin, A. S.; Jullien, L.; Hélène, C. *Nucleosides Nucleotides* **1999**, *18*, 1473–1476.
- (34) Cantor, C. R.; Schimmel, P. R. *Biophysical Chemistry*, Part II; Freeman: New York, 1980.
- (35) Garcia De La Torre, J.; Bloomfield, V. A. *Q. Rev. Biophys.* **1981**, *14*, I, 81–139.
- (36) (a) Berland, K. M.; So, P. T.; Chen, Y.; Mantulin, W. W.; Gratton, E. *Biophys. J.* **1996**, *71*, 410–420. (b) Elson, E. L.; Magde, D. *Biopolymers* **1974**, *13*, 1–27. (c) For a comprehensive review: Thompson, N. L. *Fluorescence Correlation Spectroscopy in Topics in Fluorescence Spectroscopy*, Volume 1; Lakowicz, J. R., Ed.; Plenum Press: New York, 1991; pp 337–378.
- (37) Delie, F.; Gurny, R.; Zimmer, A. *Biol. Chem.* **2001**, *382*, 487–490.
- (38) He, L.-Z.; Garamus, V.; Niemyer, B.; Helmholz, H.; Willumeit, R. *J. Mol. Liq.* **2000**, *89*, 239–249.
- (39) Israelachvili, J. *Intermolecular and Surfaces Forces*, 2nd ed.; Academic Press: San Diego, 1992.
- (40) In the present paper, the association constants are adimensional referring to the standard state: ideal solute at 1 M for the infinitely diluted solution.
- (41) Förster, T. *Modern Quantum Chemistry*; Sinanoglu, O., Ed.; Academic Press: New York, 1965; Part III, pp 93–137.
- (42) Jiang, Y.-B.; Wang, X.-J.; Lin, L. *J. Phys. Chem.* **1994**, *98*, 12367–12372.
- (43) Their morphology was not further investigated; unfortunately, satisfactory EM pictures of these objects could not be obtained.
- (44) Kuzelová, K.; Brault, D. *Biochemistry*, **1994**, *33*, 9447–9459.
- (45) See for instance: Marchi, V.; Jullien, L.; Lehn, J.-M.; Belloni, L.; Raison, D. *J. Phys. Chem.* **1996**, *100*, 13844–13856.
- (46) Breslauer, K. *Methods Mol. Biol.* **1994**, *26*, 347–373.
- (47) In absolute ethanol, for the hydroxy-terminated lipid **8**, we have  $\epsilon_8(\lambda_{\max} = 428 \text{ nm})/\epsilon_8(\lambda = 260 \text{ nm}) = 0.25$ . Upon assuming the latter ratio to lie in the same range for the chalcone conjugated to the oligonucleotide, one anticipates the fluorophore contribution to the absorption of **IGeB** and **IGeB'** at 260 nm to be less than 5% so as to justify to base the concentration determination on the DNA contribution only.
- (48) Chen, R. F.; Bowman, R. *Science* **1965**, *147*, 729–732.
- (49) Webb, R. H. *Rep. Prog. Phys.* **1996**, *59*, 427–471.
- (50) Eggeling, C.; Widengren, J.; Rigler, R.; Seidel, C. A. M. *Anal. Chem.* **1998**, *70*, 2651–2659.
- (51) Mimms, L. T.; Zampighi, G.; Nozaki, Y.; Tanford, C.; Reynolds, J. A. *Biochemistry* **1981**, *20*, 833–840.
- (52) Rigaud, J.-L.; Levy, D.; Mosser, G.; Lambert, O. *Eur. Biophys. J.* **1998**, *27*, 305–319.
- (53) Halloway, P. W. *Anal. Biochem.* **1973**, *53*, 304–308.
- (54) See for instance: Jullien, L.; Canceill, J.; Valeur, B.; Bardez, E.; Lefèvre, J.-P.; Lehn, J.-M.; Marchi-Artzner, V.; Pansu, R. *J. Am. Chem. Soc.* **1996**, *118*, 5432–5442. In fact, eq 9 requires that the total concentration in IDNA remains constant during the titration to be valid. Under the present experimental conditions, the dilution is too large to consider this assumption to be fulfilled. Consequently, fluorescence intensities were corrected from dilution before analysis. Nevertheless, this correction is not sufficient to account for the change of association extent upon changing the IDNA concentration. Therefore, eq 9 was first used to derive orders of magnitude for the association constant and for the alteration of the IDNA emission properties. Then the latter estimates were further refined from numerical simulations.
- (55) In a first step, it was taken equal to the starting concentration during the titration. See ref 54.
- (56) Krichevsky, O.; Bonnet, G. *Rep. Prog. Phys.* **2001**, *64*, 1–47.
- (57) Fukada, H.; Takahashi, K. *Proteins* **1998**, *33*, 159–166.
- (58) We noticed that the absorbance of BOBO3 slowly decreased in 100 mM NaCl, 10 mM Na(CH<sub>3</sub>)<sub>2</sub>AsO<sub>2</sub>-HCl pH 7 buffer. We supposed that BOBO3 may be hydrolyzed under such conditions. We measured the rate constants for BOBO3 degradation at different temperatures in the absence or in the presence of C/G. Results are given in Supporting Information, Figure 7S and Table 2S. They essentially reveal that (i) DNA protects BOBO3 against decomposition; (ii) BOBO3 degradation remains slow at the time scale of the present assay so as to neglect it for interpreting experimental data.